Accumulative Roll Bonding—A Review

Seyed Mahmoud Ghalehbandi [1], **Massoud Malaki** [2,*] **and Manoj Gupta** [3,*]

1   Industrial Engineering Department, University of Science and Technology of Mazandaran, Behshahr, Mazandaran 4851878195, Iran
2   Mechanical Engineering Department, Isfahan University of Technology, Isfahan 84156-83111, Iran
3   Department of Mechanical Engineering, National University of Singapore, 9 Engineering Drive 1, Singapore 117576, Singapore
*   Correspondence: massoudmalaki@gmail.com or m.malaki@me.iut.ac.ir (M.M.); mpegm@nus.edu.sg (M.G.)

Abstract: Different manufacturing processes can be utilized to fabricate light-weight high-strength materials for their applications in a wide spectrum of industries such as aerospace, automotive and biomedical sectors among which accumulative roll bonding (ARB) is a promising severe plastic deformation (SPD) method capable of creating ultrafine grains (UFG) in the final microstructure. The present review discusses recent advancements in the ARB process starting with the ARB basics, intricacies of the underlying mechanisms and physics, different materials, surface and rolling parameters, and finally its key effects on different properties such as strength, ductility, fatigue, toughness, superplasticity, tribology and thermal characteristics. Moreover, results of recent computational investigations have also been briefed towards the end. It is believed that ARB processing is an emerging area with tremendous opportunities in the industrial sector and ample potential in tailoring microstructures for high-performance materials.

Keywords: accumulative roll bonding; light-weight; composite; reinforced composite; ductility

1. Introduction

Nowadays, bulk materials with high strength to weight ratio are in high demand particularly in weight-critical industrial applications. Average grain size plays a significant role in determining the mechanical properties of almost all crystalline materials and hence ultra-fine grained (UFG) materials, i.e., materials with the sub-micron mean grain size, are widely used owing to their superior mechanical properties. In order to produce such UFG structures using severe plastic deformation (SPD) procedures, exceptionally high strain value should be considered so that a high density of dislocations can be inducted in the bulk of material resulting in re-arranged grain boundaries and new array of UFGs.

The most common SPD procedures are equal channel angular pressing (ECAP) [1], high-pressure torsion (HPT) [2] and accumulative roll bonding (ARB). ECAP can be applied to various materials where it employs simple shear without reducing cross-sectional area by pressing a metal billet through an angled channel [3–6]. HPT, however, imposes torsional/compressional stresses to a relatively small and thin metal disk [7–9], usually with no dimensional changes. Both ECAP and HPT are limited to producing small parts, relatively expensive, poor in productivity especially in continuous mass production, and usually require considerably large load capacities and dies. However, having an ability to bond similar and/or dissimilar materials, ARB is emerging as a cost-effective SPD technique to obtain large UFG sheets or multi-layered composites structures by accumulating large strains usually by repeating the procedure. It can also be easily scaled up industrially as a continuous operation. ARB is applicable for processing a large number of different materials including those that cannot be bonded by traditional bonding methods.

Invented by Tsuji et al. [10] in 1999, ARB is a solid-state multi-stage process including surface preparation, cutting, stacking, rolling and sometimes followed by a post-rolling heat treatment to improve bonding quality of the stacked sheets. Figure 1a schematically shows the process where two or more sheets are stacked together and passed through the rolls to apply plastic deformation; the deformation must be enough to produce a solid-state bonding. ARB has a great industrial potential due to a high production rate and continuous procedure. For instance, a two-layer copper/aluminum (Cu/Al) clad sheet composites manufactured by ARB can almost reduce 40% of weight, maintaining equivalent electrical and heat conductivities like a Cu alloy.
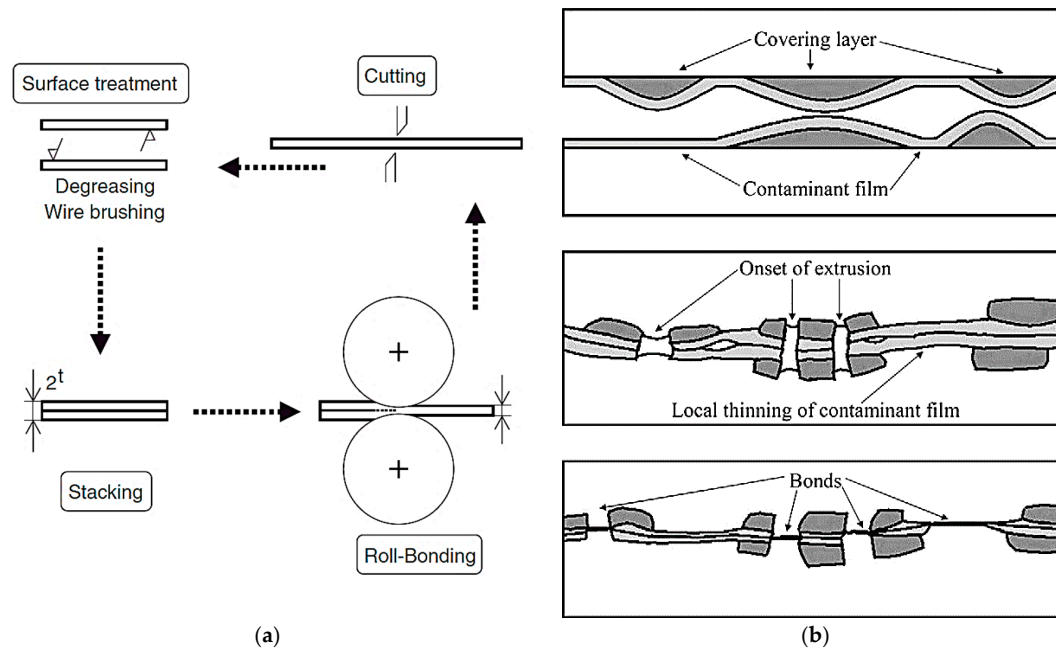

Figure 1. (**a**) Schematic illustration of principles of the accumulative roll bonding (ARB) process, (**b**) Schematic illustration of fracture and extrusion of surface layer during ARB.

The ARBed clad composites are frequently used in armored cables, yoke coils in TV sets, air-cooling fin and bus-bar conductor joints [11]. Kitazono et al. [12] employed ARB to produce a closed-cell Al foam wherein a reinforcing agent is blown between the sheets. Fattahi et al. [13] used ARB to fabricate composite filler metals of tungsten inert gas welding where the results revealed that the yield strength of welds was significantly improved when employing Al_2O_3/TiC/TiO_2 nanoparticle/Al composite filler metals. A similar effort was made by Sabetghadam et al. [14] to produce ZrO_2/AZ31 nanocomposite fillers of gas tungsten arc welding. Using ARB, Dhib et al. [15] fabricated inexpensive composites commonly used as acid containers with a low-thickness stainless steel (for inner side) stacked to a thick low-carbon metal (for outer side).

To improve bonding quality, contacting surfaces are to be degreased and wire-brushed to remove oxides or any other surface layers. As a result of rolling pressure, thickness reduction and frictions, a great amount of heat is generated wherein a synchronous presence of pressure and heat results in the bonding of cleaned surfaces. The interfacial bond is the consequence of mechanical and atomic affinity of the sheets [16,17]. To improve bonding quality, ARB can be performed at elevated temperatures or below the recrystallization temperature. Annealing heat treatment may also be considered after ARB in order to achieve strong metallurgical bonding [18–24] or improved formability [25]. The following section presents the underlying mechanisms and basic aspects.

2. Basics and Mechanisms

Bonding quality is significantly affected by ARB parameters and underling mechanisms. Ample studies have been conducted to find out the bonding mechanisms during roll bonding process. The following are four major theories proposed to explain the bonding mechanisms:

- Film theory;
- Energy barrier;
- Recrystallization
- Diffusion bonding.

Film theory proposes that if two clean metal surfaces are placed in very close contact, a bond will create. The film theory is a dominant mechanism of low temperature ARB and bonding occurs when metal surfaces are exposed and deformed to a sufficiently large value. The fracture of surface layers and extrusion of virgin metals through the cracks have the main roles in a real contact.

The energy barrier theory proposes that even if the fresh surfaces are in contact firmly, no bond creates; bonding precondition is to overcome an energy barrier. Parks concluded that the energy barrier is recrystallization; however, Erdmann-Jesnitzer believed that energy barrier is diffusion [26]. Semenov [27] suggested that the energy barrier comes from the crystal mis-orientation at the contact surfaces. His findings showed that bonding occurred for Al, Cu and silver (Ag) at the temperature of liquid nitrogen, hence it cannot be attributed to diffusion or recrystallization. Vaidyanath et al. [28] and Mohamed and Washburn [29] expressed that the film theory is the utmost mechanism during rolling at low temperatures. An appropriate surface preparation technique removes oxides and contaminant layers, creates a hardened layer, and increases surface roughness. It was expressed that brittle surface layers of both metals are broken up during the rolling operation, and the underlying layers are then exposed. The unveiled islands of metals are extruded and bonded together through opened cracks owing to rolling pressure from both sides. This mechanism has been confirmed by optical and scanning electron microscopies (SEM) [30,31]. Figure 1b depicts a simplified illustration of the film theory wherein it is showed that at the outset, fracture of the brittle top layer is ongoing when the extrusion of virgin metal has just been started through the cracks and no bonds are visible yet. Continuing the rolling operation and increasing the pressure establishes a contact between the highest asperities of the uncovered material of the two opposing surfaces to form a metallic bond. In the meantime, some other areas are uncovered and innumerable bonds are created [32]. The investigations are still ongoing to find a better understanding about the correct mechanism(s).

It should be noted that the aforesaid bonding mechanisms are metallurgical, however, it is thought that an initial mechanical bonding is first originated due to a physical contact and afterwards a strong metallurgical bond develops at the interface during ARB that may/may not be followed by a heat-treatment process [33].

3. Parameters

ARB is affected by numerous parameters from which material type, surface characteristics as well as rolling conditions are adjudged as most important. The present section identifies four distinct parameters having both significant effects on bonding quality as well as being readily controllable in practical conditions.

3.1. Materials Parameters

Material (i.e., type and extent) is likely the most important parameter in ARB. Sheet materials considered in ARB can be divided into three different categories: (i) similar materials, (ii) dissimilar materials and, (iii) similar/dissimilar materials with reinforcing agent. Based on Google Scholar, Figure 2 represents the number of documents published in the period of 1999–2018 where it is evident that early researches were almost all devoted to the ARB of similar materials. During the interval of

2007–2010, a number of researchers used the ARB for bonding similar/dissimilar sheet composites. The trend continued from 2011 to 2014, with a reduction in the bonding of similar materials and an increase in the bonding of dissimilar materials with/without the addition of reinforcements. In recent years, the number of studies devoted to ARB has grown significantly, and despite the increased attention to the bonding of dissimilar materials, attention to the bonding of similar materials has not diminished. Therefore, in the coming years, researches in this field seem to be mostly concentrated on those dissimilar bonding or the reinforced materials.
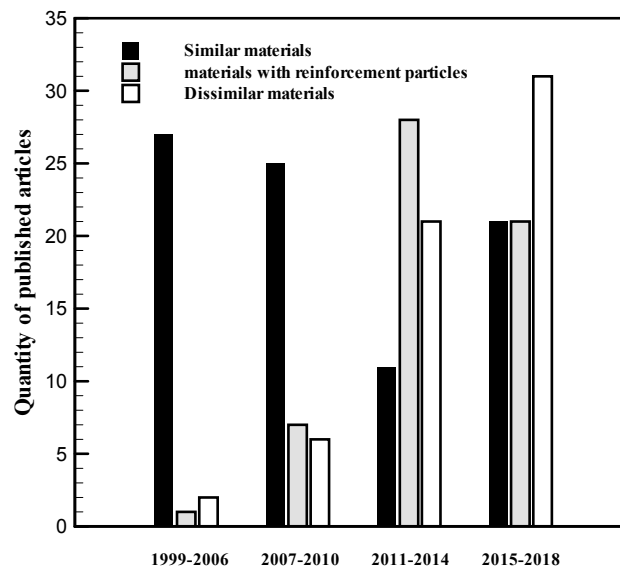

Figure 2. Trend in material selection for ARB experiments based on Google Scholar.

To date, ~50% of the experiments carried out on the ARB of similar materials have been dedicated to Al alloys; other materials in this category are steel, copper, titanium, magnesium alloys and few researches have been made on miscellaneous metals such as Mo, Zr and Ni alloys. For bonding those reinforced similar materials, the use of Al/Al alloy sheets reaches over 80%. To the best of our knowledge, one of the sheet materials is always Al or its alloys in more than 70% of ARBed dissimilar bonding process.

3.2. Surface Parameters

Mechanical strength is significantly influenced by surface characteristics in both aspects of cleanliness and roughness [34]. Metal sheets, in two stages of production and maintenance, are affected by surface contaminations disturbing nearly all surface-dependent operations. Those thermal treated sheets and the materials produced by hot forming processes possess surface contaminants, e.g., oxides. Furthermore, lubricants used in sheet metal forming processes are the other sources of surface contamination among which, grease, moisture and chemical compounds usually remain on the surface after the production, acting as bonding barriers, and hence could seriously affect the bonding quality of ARBed materials and, therefore, must be removed. It would be wrong to think that post forming cleaning processes will readily eliminate such contaminants and if they remain on the surface, it would weaken the bonding strength especially when rolling at ambient temperatures [35,36]. As a result, very careful surface preparation is required before the application of any solid state bonding operation [37]. The removal of contaminant layers from material surfaces can be performed by chemical and/or mechanical treatments.

Jamaati and Toroghinejad [38] investigated the effects of surface preparation parameters such as roughness, scratch-brushing on bonding quality. Scratch-brushing parameters encompass peripheral speed, brushing load and stiffness governing surface roughness. Shown in Figure 3a, increasing surface

roughness leads to enhanced peeling strength, and increased brittleness of surface layers that can consequently be broken easily providing more virgin layers for extruding and ensuing bonding. On the other hand, scratch brushing both cleanses and roughens the surface layers. It grants more asperities promoting localized shear deformation and breaks unavoidable oxide films during the roll bonding operation, therefore, contributing to better bonding of the two metal sheets [38–40].
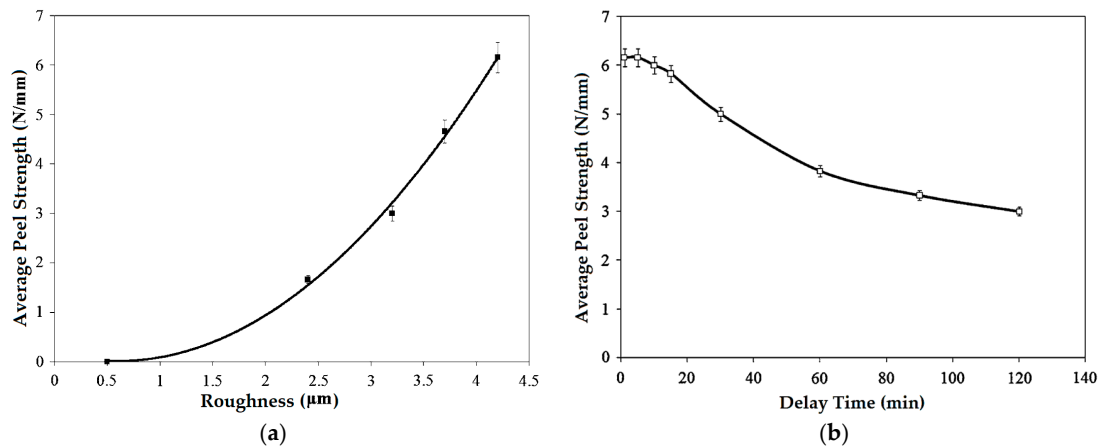

Figure 3. (**a**) Variation in average peel strength of Al strips vs. surface roughness [38], (**b**) variations in average peel strength vs. delay time [38].

There exist different surface preparation methods among which degreasing (for example in acetone) followed by scratch-brushing gives a far better bond strength. It has also been concluded that bond strength enhances, with decreasing the delay time between surface preparation operation and the consequent rolling. Figure 3b indicates that if the rolling process is carried out within the first 10 min, the bond quality is not affected, however, longer delay reduces the bond strength. Jamaati and Toroghinejad observed that the bond strength significantly decreases after 15 min of surface preparation. Also, they identified two other important parameters in scratch-brushing, namely wire diameter and length.

3.3. Rolling Parameters

3.3.1. Rolling Reduction

The main determinant to the bond quality is the plastic strain which is governed by the rolling reduction. To note that a minimum value of thickness reduction, named threshold reduction (R_t), is required to achieve sufficient bonding. The amount of R_t decreases when working temperature increases up to the recrystallization temperature. Higher than the recrystallization temperature, beneficial effects of accumulated plastic deformation are removed. If the rolling temperature is less than half of melting temperature, an acceptable bonding quality can be achieved by 50% reduction without recrystallization [41]. Qaudir et al. [42] investigated single rolling of pure Al at 300 °C and found that increasing R resulted in bonding toughness enhancement especially for those reductions greater than 47%. Similar findings were reported for Al-Cu by Yousefi et al. [36] and for Al/brass by Naseri et al. [43].

As evidence for mechanically affected bond strength, microscopic observations of Ti/Cu peeled surface at different reductions by Hosseini and Manesh [44] showed that with increasing R, the size of the surface cracks increases as a consequence of the increased surface expansion. This suggests that total cracks area and the extent of extruded virgin metals increases which leads to extended welded area and enhanced bond strength as shown in Figure 4.
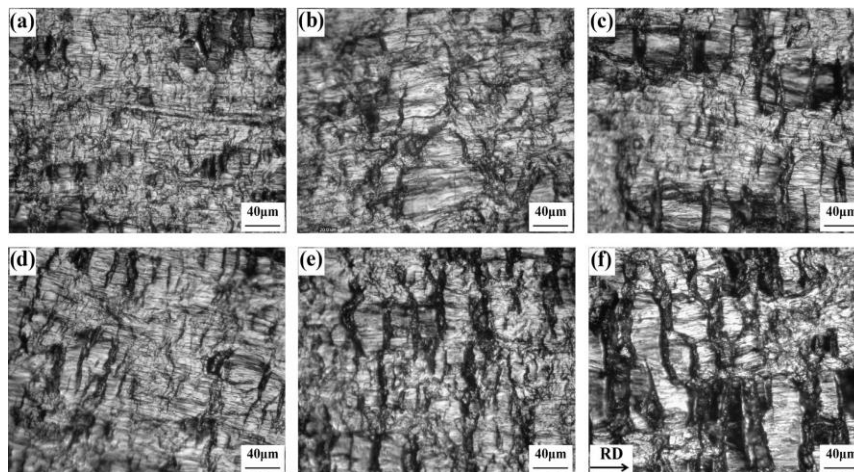
Figure 4. Optical microscope (OM) images of the Ti (**a**–**c**) and Cu (**d**–**f**) peeled surfaces, roll-bonded at the different thickness reductions of 44% (**a,d**), 56% (**b,e**) and 62% (**c,f**) [44].

As an evidence for chemically affected bond strength, Ma et al. [45] measured the diffusion layer width of ARBed Al/Ti sheets with different values of R and found that the diffusion layer width increases as R increases, thus enhancing bond strength.

3.3.2. Rolling Temperature

ARB was firstly performed at elevated temperatures [10], however, it is currently being carried out at room temperatures as well. Bonding quality is usually affected directly by temperature, i.e., increasing temperature improves bond strength through increasing diffusion layer thickness across the interfaces as shown in Figure 5a for ARBed Al/Ti samples. The rolling temperature significantly affects bonding strength and overall strength. Although the aim is to increase overall strength using temperature, it can also reduce the overall strength by activating factors such as recovery and recrystallization. Despite the fact that recovery is unavoidable at low temperatures, the rolling must be performed below the recrystallization temperature (i.e., below the half of melting point) avoiding the elimination of beneficial effects of accumulated plastic deformations. It should be kept in mind that if the other involving parameters, such as material and reduction percentage, cause a high quality bonding between the sheets without increasing the temperature, the final strength will be greater due to the reduction of the aforementioned deteriorating factors.
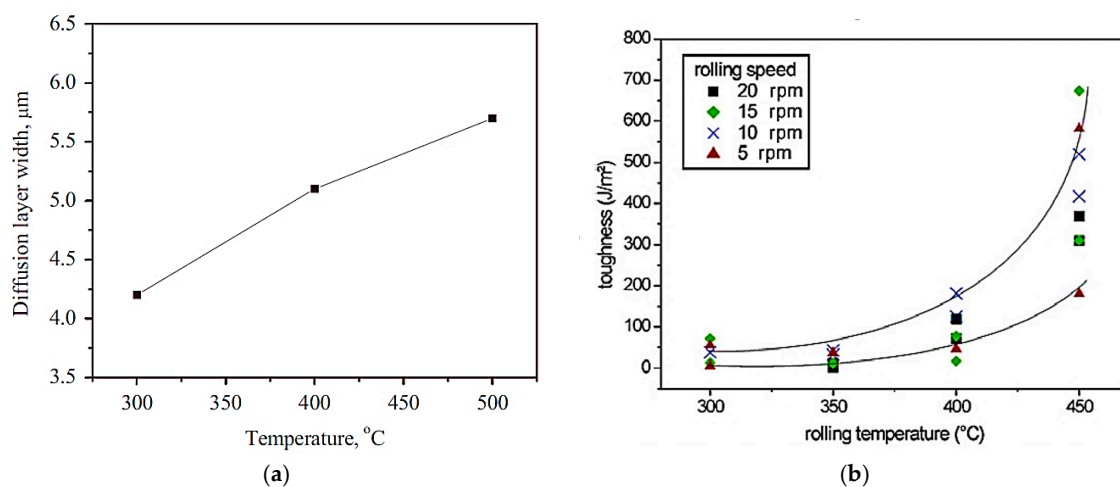
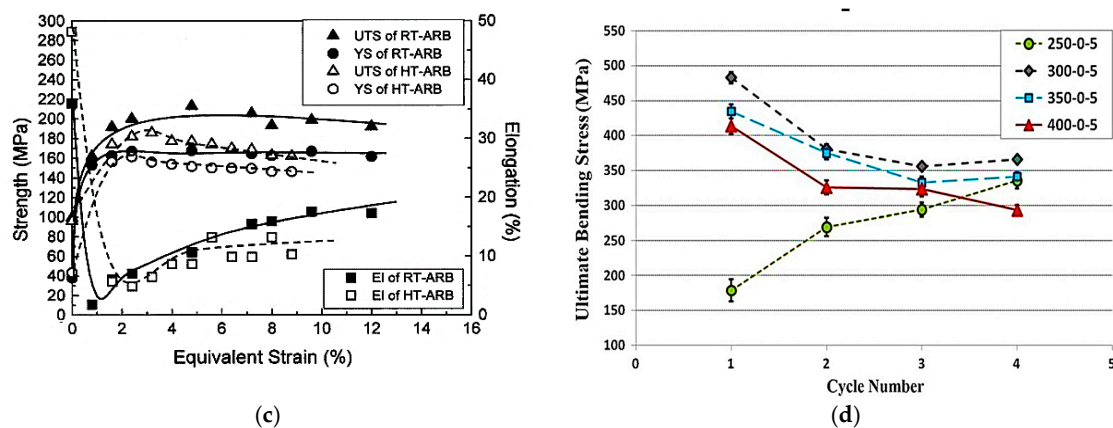

(a)

(b)

Figure 5. *Cont.*

(c)

(d)

Figure 5. (**a**) Variation in diffusion layer width with rolling temperature for ARBed Al/Ti sheets [45], (**b**) Influence of both rolling temperature and roll speed on bond toughness of Al strips [42], (**c**) Variation of ambient tensile properties of 8011 alloy with increasing the equivalent strain in RT-ARB and HT-ARB samples [46], (**d**) Ultimate bending strength of the ARBed Al/AZ31 at different temperatures [47].

Quadir et al. [42] studied the peeling behavior of ARBed Al sheets where an increase in ARB temperature leads to an increase in bond strength in term of toughness (Figure 5b). They emphasized that a continuous elevation in bond strength does not guarantee a continuous improvement in overall strength; i.e., performing ARB at higher temperatures (especially above recrystallization temperatures) may lead to a reduction in final strength. Xing et al. [48] reported the effect of rolling temperature on final strength of ARBed AA8011 where they showed that after the strains of ~4.8 at room temperature, the ultimate tensile strength (UTS) of ARBed samples started to decrease due to dynamic recovery. For HT-ARB specimens preheated at 200 °C before each cycle, dynamic recrystallization and static and dynamic recovery may cause a reduced UTS at lower strains and also lower strength compared to those samples rolled at ambient temperature. Zhan et al. [46] also observed a reduction in the final strength of ARBed AZ31 alloy with increased rolling temperature (Figure 5c). Also, Abbasi and Sajjadi [47] studied both aspects of the rolling temperature effects on mechanical strength wherein the bending behavior of ARBed Al/AZ31 sheets rolled at different temperatures was examined. As shown in Figure 5d increasing the rolling temperature from 250 to 300 °C enhanced the bending strength; however, further increase to 350 and 400 °C resulted in a reduction due to the recrystallization and microstructural refinement.

3.3.3. Rolling Speed

Decreasing the rolling speed usually results in stronger bonding because the bonding quality is greatly affected by the diffusion of adjacent materials and the time of synchronized contact-pressure. Depending on material type, surface features and rolling temperature, there might therefore be a threshold value of rolling speed above which an acceptable bonding is not guaranteed. As shown before in Figure 5b, Quadir et al. [42,49] investigated the effect of roll speed on strength of Al strips at elevated temperatures. While scattered data was produced at high rolling temperatures, the effects of rolling speed on bond strength are undeniable, therefore, data presented so far cannot provide a definite relationship between strength and roll speed and it needs further investigation since it has a significant influence on production time.

3.3.4. Rolling Friction

Most of ARB researches have been performed without lubricants. Shown in Figure 6a Jamaati and Toroghinejad [32] performed ARB at different friction coefficients with lubricant, and in dry and rough surface conditions where the average peel strength increased when the friction coefficient increased

between the strips and rolls probably due to the increased mean contact pressure between the outer layers and the rolls.
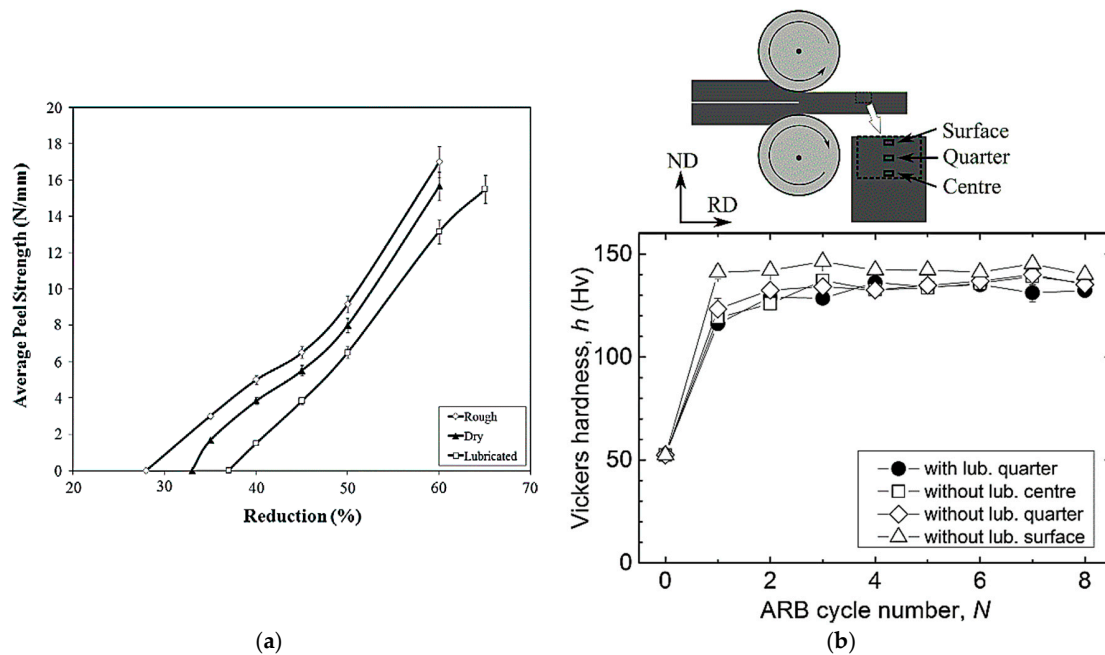

Figure 6. (**a**) Average peel strength versus the reduction in three frictional conditions, i.e., rough, dry and lubricated surface conditions [32], (**b**) Hardness of ARBed 4N-Cu with and without lubrication [50].

The effect of lubricant on mechanical properties of ARBed Cu was studied by Miyajima et al. [50] where they concluded that, if the surface friction is reduced by lubricant, the deformation is treated as a plane strain compression, of which equivalent strain is about 0.82; nonetheless, higher frictions usually exert larger strains adjacent to the surface and hence enhance microstructural evolution close to the surface being described as an additional shear strain. The additional shear strain is mostly created on the surface, so the corresponding effect is more pronounced at this region. Of course, it should be noted that additional shear strain still exists inside the ARBed materials as the central points were at surface points before the last roll bonding steps; finally, grain refinement was accelerated in case no lubricant was used due to the additional shear strain [50].

As shown in Figure 6b, at earlier ARB cycles, hardness value increases to ~140 Hv at surface layers when no lubrication is consumed; the hardness of the other samples reaches to ~120 Hv. The hardness at the surface of ARBed sample without lubrication seems to be constant, whereas for the other sections (center and quarter) increases gradually with increasing cycle number and then saturate. The reason why the hardness at surface layers is almost always higher than those of inner regions is due to the additional grain refinement caused by the friction between the sheets and rolls.

3.3.5. Number of Layers

Regarding the number of stacked sheets, Jang et al. [51] investigated the strength of ARBed 2- or 3-layer Cu sheets wherein tensile strength is dominantly determined by applied equivalent strain as well as the materials strength; ARBed samples followed a similar trend up to a critical point. Past the mentioned critical point, tensile strength is solely determined by the dynamic recovery rate under SPD conditions. Regarding the number of layers, Lee et al. [52] observed a similar behavior for IF steel. They also studied the effects of post ARB annealing on strength. According to Figure 7, besides the gradual decrease in the strength during annealing, they stated that the decrease in strength with annealing is larger in six-layer stack ARBed specimen than in two-layer stack ARBed one and attributed this to the difference in total strain (or stored energy) where the amount of total strain was larger in the

six-layer stack ARB comparing to the two-layer one. Therefore, the released energy during annealing would be larger in the six-layer stack ARBed sample, resulting in larger decrease in the strength during annealing treatment.
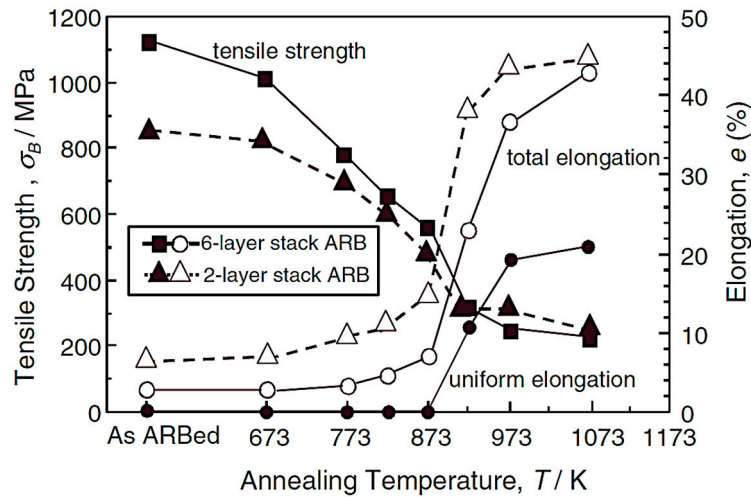

Figure 7. Changes in mechanical properties with annealing temperature of IF steel processed by three cycles of six-layer stack ARB compared to the results of a two-layer one [52].

3.3.6. Reinforcement Particles

From a perspective, the sheets produced by ARB, can be divided into monolithic, composite and metal matrix composite (MMC) forms; the latter is usually produced with the addition of reinforcing agents. Using ARB, MMCs can be produced by uniform distribution of strengthening additives between the sheets. The effect of these additives in terms of shape, geometry, size, material, and volume fraction can be investigated. Alizadeh and Paydar [53] studied the effects of SiC particles on the mechanical properties of Al strips. At first, they used a peeling test to find out the effect of carbide particles on the bond strength and also to measure the minimum reduction required for achieving an acceptable bond between the two strips. For one-cycle ARBed specimens, their results are presented in Figure 8a,b. The results show that SiC decreases peeling force at constant reduction since SiC prevents the extrusion of virgin material through interfacial cracks; therefore, bonding area and consequently bond strength decreases. As a result, while using SiC, the bonding is not successful unless thickness reduction is sufficiently high, i.e., 66% (with SiC) and 50% (without) reductions in thickness are required. In addition, their results showed that reinforcement would reduce the bond strength in the first ARB cycle. Shown in Figure 8c,d, it was concluded that the UTS of the Al/SiC$_p$ metal matrix composite can be improved by increasing the number of rolling cycles up to seventh cycle; it is then saturated for higher cycles. The microstructural evaluation indicates that by increasing the number of cycles, the uniformity of SiC particles increases and porosity decreases.

Another observation made by researchers was that the Al/SiC$_p$ composite specimen exhibit lower strength than the monolithic one before three ARB cycles, which confirms the fact that for an acceptable composite production using ARB a minimum number of cycles is necessary to decrease the amount of porosity and to reach a balanced distribution of particles in the metal matrix. Although SiC addition had a positive effect on the strength of ARBed specimens, the elongation to failure decreased.
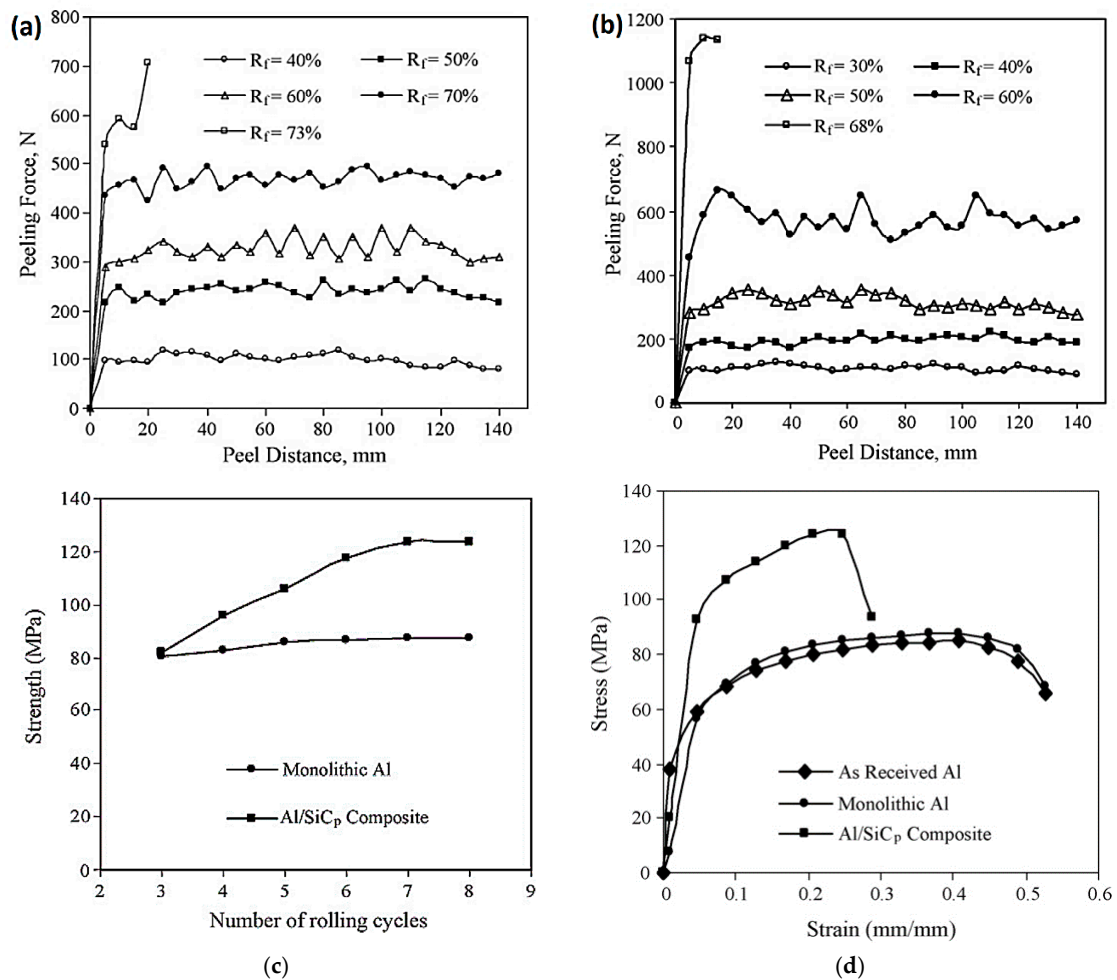
Figure 8. Variation of peeling force in ARBed Al-1050 strips, (**a**) in presence and (**b**) in absence of SiC particles [53], (**c**) tensile strength of composite and monolithic samples versus number cycles and (**d**) stress–strain curve of as received and ARBed samples after seven cycles [53].

Rezayat and Akbarzadeh [54] examined the effect of alumina particles on the R_t of pure Al sheets (Figure 9). They indicated that R_t increases to 45% in the presence of the alumina particles compared with the R_t of 20% being needed for the bonding of Al sheets under the same conditions attributing it to the friction coefficient reduction and the need for longer channel extrusion of virgin metal surfaces through the cracks in the presence of a powder layer.

Jamaati and Toroghinejad [55] investigated the effect of volume fraction on the strength of MMCs produced by ARB for pure Al reinforced by different weight percentages of anodized Al strips. Besides the strength enhancement provided by the SPD, mechanical strength could be significantly improved by reinforcing alumina particles used in the host material. It should be noted that strain hardening and dislocation strengthening play a key role in strength enhancement for ARBed monolithic specimens. For the reinforced ARBed MMC specimens, the particles act as a barrier against dislocation movement and crack growth. Similar result for the enhanced strength with increasing volume fraction of particles has been reported in all researches conducted on the ARB produced composites [56–58]. Liu et al. [56] showed that after increasing the volume fraction of tungsten by 2.8%, further increase in strength is not realized [59].
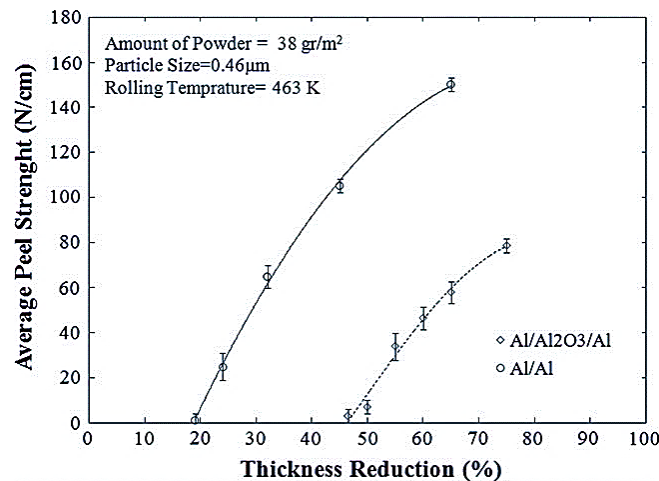
Figure 9. Average peel strength versus the thickness reduction [54].

Jamaati et al. [60] studied the influence of particle size on the properties of ARBed IF steel composites using SiC micro- and nano-particles. Figure 10 demonstrates that the tensile strength of MMCs containing nanoparticles is far better than those strengthened by microparticles owing to extremely higher matrix/reinforcement interfaces in nanoparticles, and hence leading to higher local dislocation density, refined grain size and improved mechanical performance. Furthermore, particle breaking is a damaging factor where larger particles tend to crack more readily and composites with microparticles display reduced strength. Also, hardening effects might be important as the length scale of the stress inhomogeneities, which are on the order of the particle size, is analogous to typical microstructural lengths.
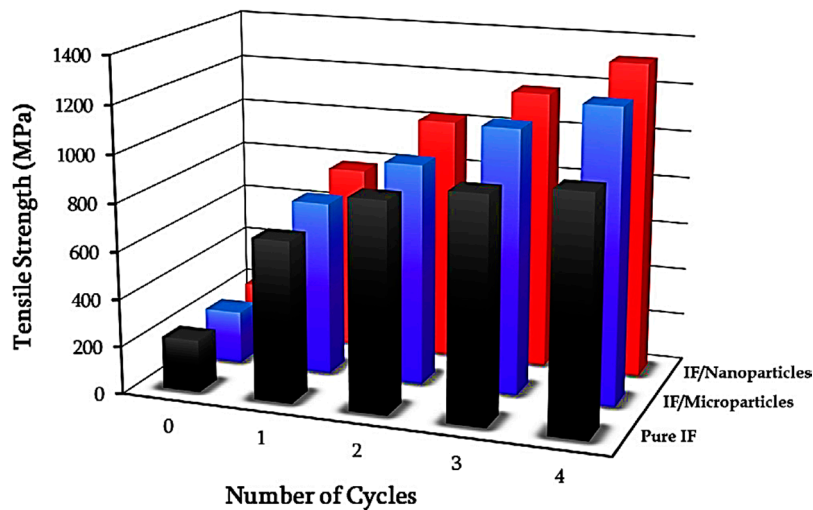

Figure 10. Tensile strength of ARBed pure IF steel, composite and nanocomposite versus number of cycles [60].

In spite of extensive research on the aforementioned parameters, the effect of other rolling parameters, such as rolling direction, layer thickness and roll diameter, on the properties of ARBed sheets have not yet been fully understood and further research are required in this area.

3.3.7. Post-Heat Treatment

The formability of ARBed materials is generally poor due to limited ductility. To address this problem, post ARB heat treatment is a viable choice. For materials deformed more than a certain

level of strain, a transition in annealing behavior occurs from the conventional recrystallization (i.e., nucleation and growth), typically observed for samples deformed to medium/large strains, to a process of extended recovery, where a continuous microstructural coarsening is observed [61,62]. Strain has a significant effect on the recovery rate of those materials deformed by very large values of strain. A fast recovery rate in the form of structural coarsening may enhance nucleation; nevertheless, the fast structural coarsening in the material around any nuclei reduces the driving force for its growth, i.e., a competitive effects between the growth of nuclei and the structural coarsening that might be influenced by different parameters, e.g., processing conditions, solute content, intermetallics, as well as annealing treatment parameters [63].

Sheng et al. [11] evaluated the influence of annealing treatment on the interface of Cu/Al composite fabricated by one-cycle cold rolling. As shown in Figure 11, it is clear that an appropriate heat treatment may greatly improve bonding quality and high bond strength can be achieved (annealing at 423 K for 20 h). In fact, relatively low annealing temperature and short time heat treatment significantly improves the bond strength. On the other hand, the strength drastically reduces at higher annealing temperature or longer treating time due to the growth of brittle intermetallic compounds that deteriorates the ductility of final products. It was also shown in other research [64] that the formability of ARBed sheets are enhanced by annealing to realize both recrystallization and interlayer diffusion.
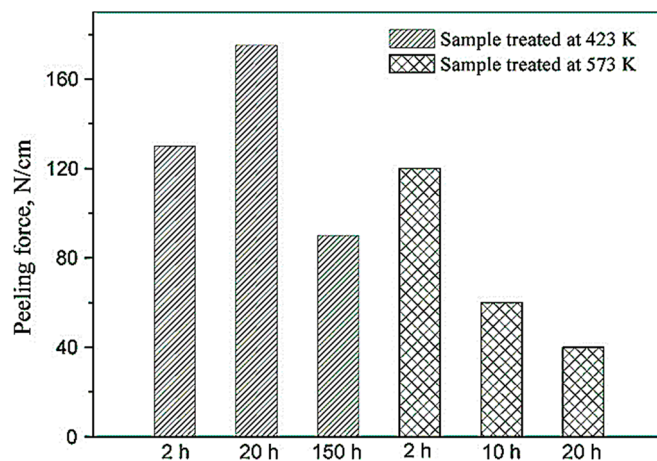

Figure 11. Peeling force of Cu/Al/Cu clad sheet with different heat treatment temperatures or times of heat processing [11].

Some studies used post ARB aging process as a way of enhancing the strength of age hardenable sheets. For example, Rezaei et al. [65] investigated the mechanical properties and microstructural features of ARBed 6061 Al followed by ageing treatment and reported that both the UTS and elongation values increased after an ageing operation at two temperatures (337 K and 437 K) for different rolling cycles (i.e., 0–5 cycles). The results obtained revealed the competing effects of recovery and precipitation involved during the ageing process, i.e., dislocation density decreases due to recovery while precipitation occurs during the ageing contributing to the UTS enhancement and strain hardening. Based on the results obtained, it was shown that the contribution to strength improvement by precipitation is higher than the loss of strength due to recovery as both the UTS and elongation values were enhanced.

4. Properties

Bond strength and peeling strength are the two most important properties recognized for ARBed samples while other characteristics such as superplasticity, damping, wear, corrosion, cyclic behavior as well as chemical, physical and thermal behaviors have also been reported in the literature. In the present section, mechanical behaviors of ARBed materials are discussed.

4.1. Strength and Ductility

Measuring yield stress (YS), ultimate tensile strength (UTS) and elongation (El) are the basic indicators of strength and ductility of ARBed materials. Since there are some differences in strengthening mechanisms of similar, dissimilar and reinforced sheet materials during ARB, the effect of ARB on strength and ductility is discussed in three different sections.

4.1.1. Sheets with Similar Materials

As mentioned earlier, improved strength and reduced ductility usually occurs after the ARB process; however, Xing et al. [66] investigated ARBed AA8011 at elevated temperatures wherein the YS and UTS only increased up to 2 cycles and then decreased; in contrast, the elongation diminished up to 2 cycles and then increased. Strengthening AA8011 alloy can be attributed to solid solution hardening, precipitation hardening, grain refinement and strain hardening. It was reported that dynamic recovery and static recovery easily takes place in Al–Fe alloys and the microstructural evaluations of AA8011 disclosed that the grain refinement contributes to strength enhancement only after the first cycle. The precipitation of Si particles was found to be an effective strengthening factor for AA8011 at 200 °C, nonetheless, a reduction in the concentration of precipitates may lessen the strength after a specific amount of precipitations probably leads to a decrease in strength with increasing ARB cycles. Having the ability of precipitation hardening, dynamic and static recovery may be considered as weakening factors for high cycle ARB, confirmed by these researchers later in another research work where they scrutinized the ARB of AA8011 at room temperature and observed that increasing the number of cycles resulted in the increased strength [48]. Hence, increasing or decreasing strength or ductility by increasing the cycles is affected by the competing effects of the strain hardening and grain refinement on one side and the recovery on the other side.

Similarly, with an increase in tensile strength after each ARB cycle, abrupt decreases in elongation after the first cycle are reported for alloys like AA6061 [67,68], AA1100 [69], AA5083 [70], AA1050 [71] and Mg alloy [72]. Similar to Al8011, however, a gradual increase in elongation after initial cycles is reported, suggesting that the strain hardening can not solely explain the mechanical properties variation observed for the ARBed metals and alloys; instead, it is caused by dynamic and probably static recovery of a heavily deformed structure. In addition, the aforementioned behavior is also reported for Cu and its alloys [73,74], AA5052 [75], AA6014 [76], AA7075 [77], AA2024 [78] and pure Ti [79–81]. It is noteworthy that few articles have also reported simultaneous improvement in strength and ductility. Naseri et al. [82] proposed a new strategy for the simultaneous increase in both strength and ductility of AA2024 where after each ARB cycle, an annealed AA2024 strip is laid between the two roll-bonded strips resulting in a composite with a bimodal microstructure consisting of coarse and ultrafine elongated grain structures.

4.1.2. Sheets with Dissimilar Materials

Based on the search made by the authors, although Zhang and Acoff [83] first produced ARBed dissimilar materials, the first seminal study on the mechanical properties of ARBed composite sheets seems to be reported by Eizadju et al. [84], where the mechanical properties of multi-layered Al/Cu composite were investigated. The main goal was to fabricate an ARBed Al/Cu composite with better mechanical properties than those achieved from ARBed Al or ARBed Cu only. Demonstrated in Figure 12, the strengths of both ARBed Al/Al and Al/Cu composites have a striking increase compared to the commercial pure Cu and Al. In contrast, elongation of ARBed samples has considerably decreased compared to pure samples. It was noted that Al/Cu composites demonstrate higher strength than ARBed Al/Al while the elongations are almost the same.
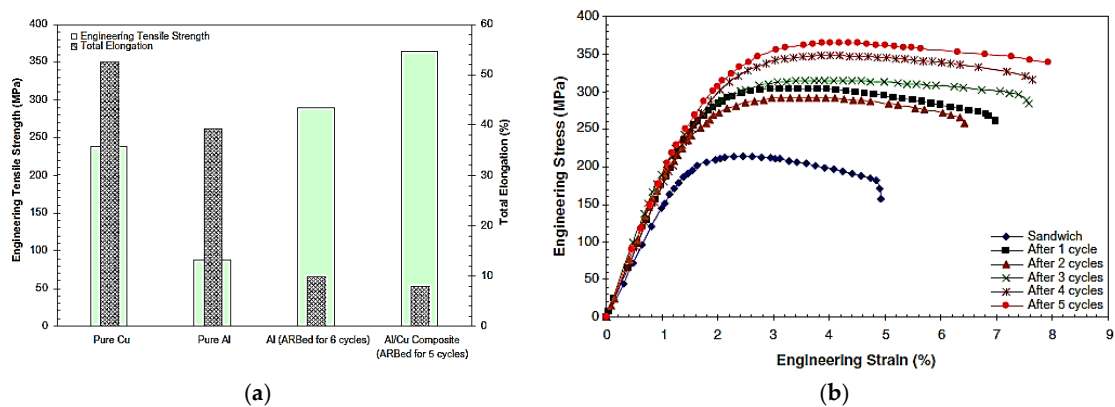
Figure 12. (**a**) Yield strength and total elongation of Cu, Al, ARBed Al, and ARB Al/Cu composite, (**b**) engineering stress–strain curves for ARBed Al/Cu composite with cycles [84].

As seen, the strength varied considerably after each ARB cycle where the variations are controlled by two main strengthening mechanisms; i.e., strain hardening by dislocations and grain refinement. In the early cycles, work hardening was the proponent, while in higher cycles, UFG structure appeared to have a dominant strengthening role. Like other ARBed materials, elongation usually decreases intensively after the first cycle due to the reduced dislocation mobility as well as few shear bands [85]. With an increasing number of cycles after the first cycle, elongation increases due to increase in bond strength between matrix and reinforcement, since the Cu layers act as reinforcement due to their fracture during higher ARB cycles as can be seen in Figure 13. A similar trend in changing strength and elongation during ARB cycles is reported for Al/Ti [86], Al/Zn [87], Al/Ni [88], Cu/Ni [89] and AA1050/AA6061 [90] ARBed composites.
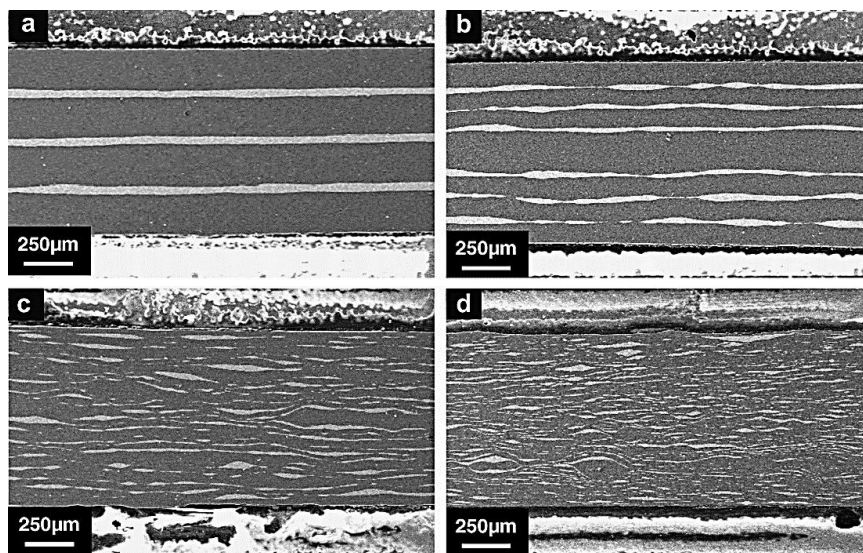

Figure 13. Scanning electron microscope (SEM) micrograph of ARB processed Al/Cu composite cross sections (**a**) primary sandwich, (**b**) 1st cycle, (**c**) 2nd cycle and (**d**) 5th cycle [84].

Sun et al. [91] studied the ARBed Cu/Zr multi-stacks and could achieve an enhanced tensile strength as ARB cycles increased due to microstructural refinement. As shown in Figure 14a, the elongation improved up to six cycles and then decreased with further increase in number of ARB cycles. For those samples processed for less than six cycles, fractography revealed formation of successive cracks along the interface between the Cu and Zr layers due to the inhomogeneous microstructure and strength differences between Cu and Zr. Zr is relatively hard and therefore only Zr layers sustain the

external load and thus fracture quickly after the yield point. Different deformation behaviors lead to the separation of dissimilar layers; nonetheless, the mentioned mechanical difference gradually reduces and this considerably postpones final failure. As a result, the elongation moderately increases to reach a maximum value at six cycles. Similar trend has been reported for Al/Zn [92] and Al/Cu/Mn [93]. ARBed composites, however, still further research is required to investigate ARB of dissimilar materials since inconsistent trends are sometimes reported related to the strength and elongation variation [94–96].
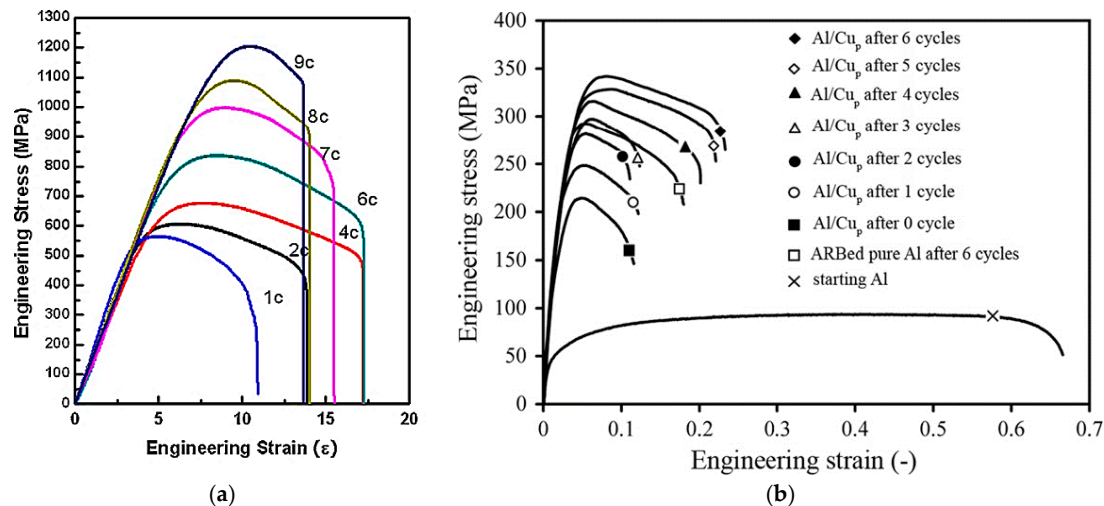

Figure 14. (**a**) Variation of stress–strain curves of the ARBed Cu/Zr materials versus ARB cycles; elongation increases up to six cycles [91], (**b**) engineering stress–strain curves for starting Al, ARBed pure Al after sixth cycle and Al/Cu$_p$ composite within different cycles of ARB process [97].

4.1.3. Sheets with Reinforcements

Metal matrix composites (MMCs) can be synthesized using ARB method by placing reinforcing agent between the sheets. Kitazono et al. [12] initially used ARB to produce Al foams by dispersing particles between Al sheets. Cheng et al. [98] and Alizade and Paydar [53] used ARB to produce MMCs. Amirkhanlu et al. [99] produced Al/Al$_2$O$_{3p}$ cast composite and Ardakani et al. [100] fabricated Al/SiC$_p$ composite, both reporting simultaneous enhancement in strength and ductility with increasing ARB cycles. It should be noted that strengthening mechanisms of the ARBed composites are not exclusively limited to those mentioned earlier for other types of ARB, i.e., ARBed similar or dissimilar sheets; however, they are also attributed to the following items:

a. Reinforcement particles acting as barrier against dislocation movement. The first mechanism is the strengthening effect since adding reinforcements to a metal matrix significantly improve mechanical strength due to dislocation pile up around the particles [101,102].

b. Improved uniformity of reinforcements. When the reinforcement distribution becomes more uniform and homogeneous, the stress concentration sites reduces enhancing the mechanical response [103,104].

c. Improved bonding quality at the matrix/particle interfaces. Regardless of volume fraction, size, shape and the spatial distribution, the mechanical property greatly depends upon how well externally applied load is transferred to reinforcing materials, i.e., stronger interfacial adhesion enhances load transfer capacity leading to improved mechanical performance [105]. Better interfacial adhesion may be obtained through increasing ARB cycles [53]. Also, porosity may have detrimental effects on bonding quality between the reinforcing agents and the host matrix where the interfacial adhesion may be lowered by porosity causing interfacial debonding. When pores are located at the particle-matrix interface, particles are debonded from the matrix even

under low stress [106]. Last but not least, porosity tends to reduce effective cross-section area and hence adversely affect mechanical strength [107].

Using reinforcing particles in the ARB process has an ability to enhance mechanical strength. For instance, Alizade and Talebian [97] compared ARBed Al/Cu$_p$ with monolithic Al where a significant improvement in both strength and ductility was observed (Figure 14b). Increasing ARB cycles further enhanced strength and ductility due to increased adhesion strength between the Al matrix and Cu particles. Moreover, the ARB process boosted the uniformity of Cu clusters and could limit the porosity as confirmed by microstructural investigation. Similar trend was seen for the ARBed Al 5083/SiC$_p$ [108], Al-Al$_2$O$_3$/SiC$_p$ [59,109], Al-Al$_2$O$_3$/B$_4$C$_p$ hybrid composite produced by anodizing [110], coated Al–Cu–25Ni/SiC$_p$ [111], Al-Al$_2$O$_3$/ZrC$_p$ [112], Cu/Graphene$_p$ [113] and Al/Al$_2$O$_{3p}$ [114] where significant strength improvement as well as increased ductility are simultaneously reported. According to Rezayat et al. [115], alumina particles enhance the YS, UTS and the elastic modulus, but the elongation falls drastically attributing mostly to plastic zone created around the reinforcing particles.

4.2. Thermal Stability

Heat treatment such as annealing process may considerably improve the mechanical properties of ARBed materials if appropriate temperature and time are chosen, particularly for SPDed materials with high level of stored energy. Intensive grain growth and loosing UFG structures are the results of improper annealing.

Park et al. [116] investigated the thermal stability of ARBed 6061 Al alloy where the grain size and microhardness were studied at different annealing temperatures. It can be seen in Figure 15 that grain size and hardness were relatively unchanged and uniformly distributed below the annealing temperature of 473 K. In contrast, for the samples annealed at temperatures above 473 K, bimodal grain size was observed including coarse grains and UFG. Considering the low activation energy of grain growth for the ARBed specimens, they emphasized that the non-equilibrium characteristics of grain boundaries of UFG alloy leads to the existence of ill-defined grain boundaries; hence, it can be postulated that the thermal stability of the ARB produced UFG materials depends mostly on the state of the SPD microstructure.

Slamova et al. [117] studied the thermal stability of ARBed Al-Fe-Mn-Si sheets at elevated temperatures (see Figure 16) using the hardness as a function of annealing temperatures. In all specimens, the hardness remains nearly constant at annealing temperatures of <200 °C, but then drops more rapidly, especially for cold-rolled specimens. The different annealing responses of ARBed and cold-rolled samples might be justified by discrepancies in stored deformation energy providing driving force for recrystallization. Furthermore, the nucleation and growth of new grains are more rapid in cold-rolled samples than that of elevated temperature ARBed ones.

For ARBed samples roll bonded at 250 °C, the most pronounced reduction in hardness occurs at 250 °C in the specimen with six ARB cycles, whereas in the one with two cycles, a gradual hardness diminution is observed when the annealing temperature is raised within the range 200–350 °C. In contrast to the ARBed specimens with two cycles, the sheets roll bonded by six ARB cycles required a considerably higher temperature of 450 °C to achieve fully softened material. In the specimens roll bonded at 350 °C, the greatest drop is shifted to 350 °C, therefore, softening due to the annealing treatment of the ARBed samples depends on the strain induced by the ARB as well as the recovery influenced by the ARB temperature. The results of the hardness measurements thus indicate that the ARBed stacks processed at 350 °C or by six cycles at 250 °C are most thermally stable.
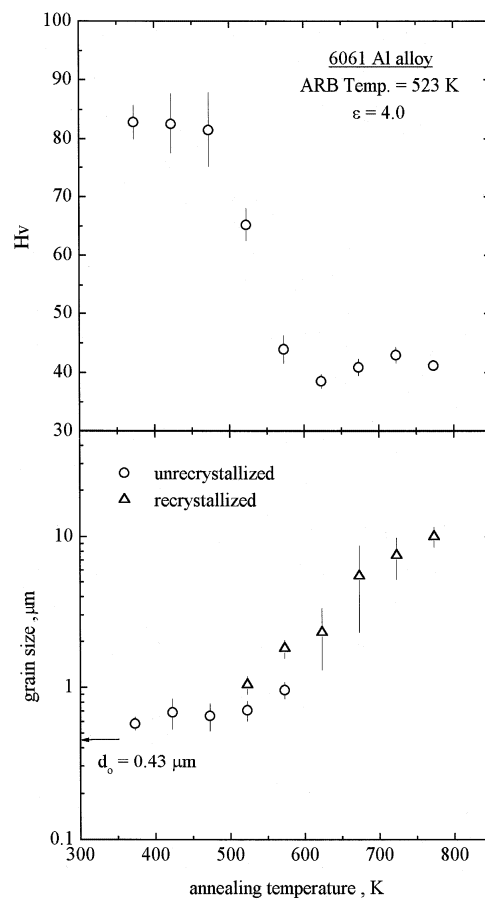
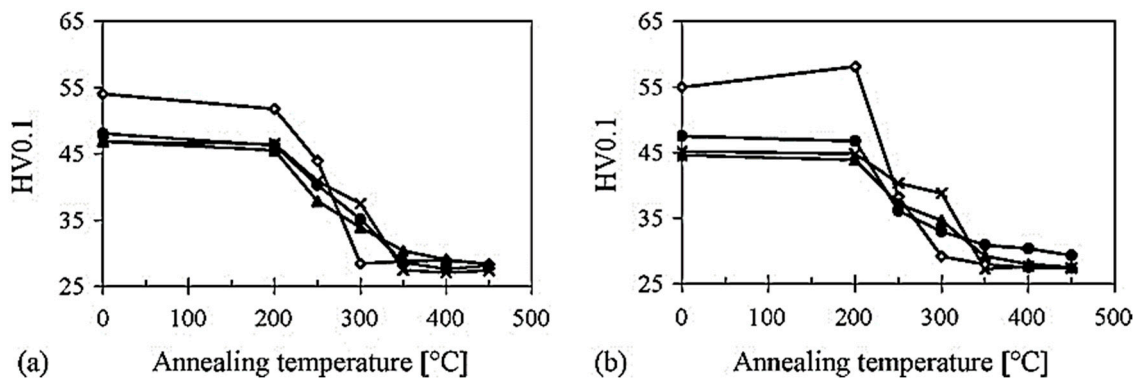**Figure 15.** Grain size and microhardness of ARBed 6061 Al alloy under different annealing temperatures [116].

Figure 16. Hardness versus the annealing temperature of ARBed Al-Fe-Mn-Si sheets with (**a**) two cycles, (**b**) six cycles at 250 °C (■), 300 °C (▲) and 350 °C (×) and in cold-rolled condition (◊) [117].

4.3. Superplasticity

Despite the fact that the main property of the ARB materials is the significant improvement in the static strength, it is also expected that the resulting UFG product may exhibit improved superplastic deformation behavior. In 1999, Tsuji et al. [118] who invented ARB, published research regarding the superplasticity of ARBed Al–Mg alloy. Constitutive relationship in superplasticity indicates that grain refinement would result in both an increase in strain rate and a decrease in superplasticity temperature, so it can be concluded that the ARB improves superplastic deformation behavior. Their results indicated low temperature superplasticity due to ultra-fine grain refinement after ARB.

4.4. Damping

Having both high damping capacity and high strength is important for structural materials that are subjected to dynamic loading conditions; nonetheless, an increase in damping is usual accompanied by a decrease in strength. It is evident that the SPD produces high strength metals through producing UFG microstructures, furthermore, severely deformed materials typically contain innumerable lattice defects giving rise to internal friction or material damping. Having a high density of grain boundaries formed by SPD is another reason for UFGed materials to have high damping properties.

Koizumi et al. [119] investigated the damping capacity of ARBed UFG Al samples where a torsional pendulum apparatus was used to measure the internal friction values versus the strain amplitudes. Both ARBed pure Al sheets exhibited high damping capacity as well as high strength attributing to the vibration of the dislocations whose ends are tightly bonded with grain boundaries of the ultrafine grains and hence could attenuate vibrational energies. Emadoddin et al. [120] explored the damping behavior of ARBed Al/SiC$_p$ multilayer composites and extracted the first-mode damping capacity as a function of amount of reinforcing particles(Figure 17). Increasing the amount of reinforcement led to increased damping capacity and that the obtained values of the reinforced samples were greater than monolithic Al6061 alloy specimens due to internal friction caused by SiC and its accompanying modification effects on the matrix microstructure. Based on the microstructural studies, a lot of holes, detachments, weak imperfect bonding were observed at the interface between the reinforcements and the host metal matrix, all contributing to damping capacity enhancement [121]. It was also found that increasing ARB cycles, the number of layers, thickness reduction ratios and temperatures leads to better damping capacity [120].
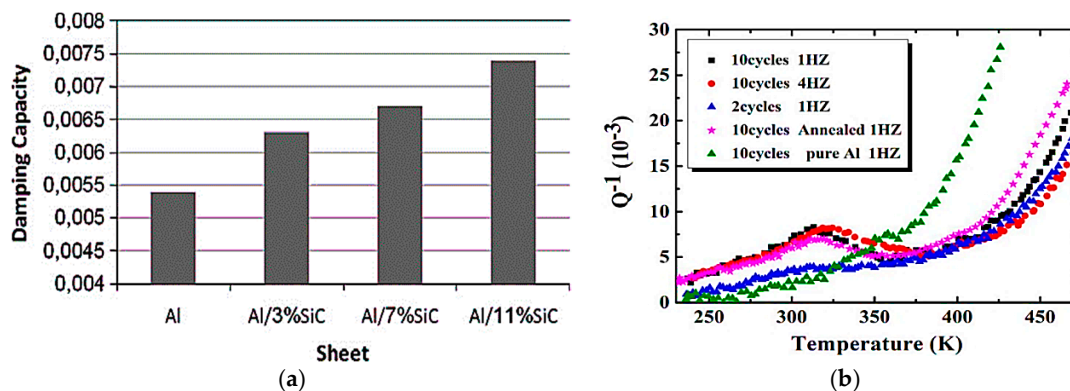

Figure 17. (**a**) First mode damping capacity of sheets with different percent of reinforcing agent [120]. (**b**) Damping capacity of Al/LLZNO$_p$ composites at different temperatures and ARB cycles [121].

Zheng et al. [121] studied the damping capacity of ARBed Al/LLZNO$_p$ composites at different temperatures where the damping capacity improved when the ARB cycles increased reaching its highest value after 10 ARB cycles at 320 K, being 4.5 times higher than that of monolithic samples. They attributed the increase in damping capacity to the uniform distribution of LLZNO particles and better bonding strength between the particles and the matrix material.

4.5. Fracture Toughness

UFG materials processed by ARB may not be applied in industrial applications if they exhibit poor fracture response. Research on the fracture behavior of UFG structures reports that different materials exhibit varied fracture behaviors, i.e., it could improve or reduce after a SPD operation. Rahmatabadi et al. [122], for the first time, experimentally evaluated the ARB effects one the plane stress fracture toughness of Al 1050 and showed that the values of fracture toughness improves by increasing the number of ARB cycles. As shown in Figure 18, fracture toughness reaches to a

maximum value of 25.4 MPa.m$^{1/2}$ after performing seven cycles, i.e., 155% enhancement compared to the annealed specimens.
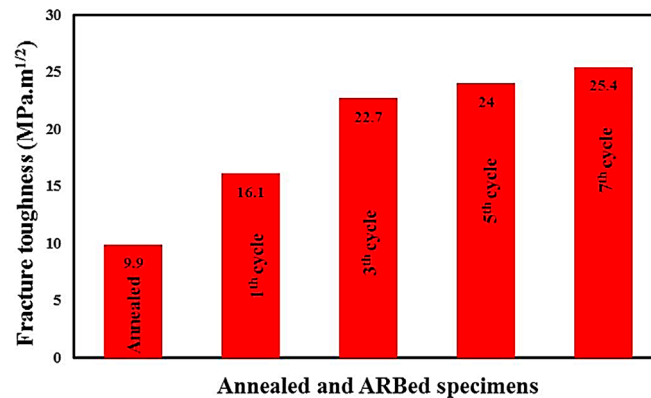

Figure 18. Plane stress fracture toughness of the ARBed Al 1050 specimens for different cycles [122].

Strength and ductility are the main influencing parameters on fracture toughness. In initial ARB cycles, the effect of strength enhancement is more pronounced than the ductility reduction; then the ductility reduction becomes severe. However, after an ample rise in ARB cycles, ductility values are resumed again and therefore, fracture toughness re-increase [122–124].

4.6. Wear

Wear properties can be tailored using ARB process to meet the end tribological requirements. Talachi et al. [125], observed that the wear rate of ARBed pure Al sheets increases gradually with ARB cycles as shown in Figure 19. The wear resistance was increased up to the third cycle due to hardness increase and then reduced due to poor strain hardening capability [126]. The wear rate increment at the first cycle can be attributed to decreasing ductility [85].
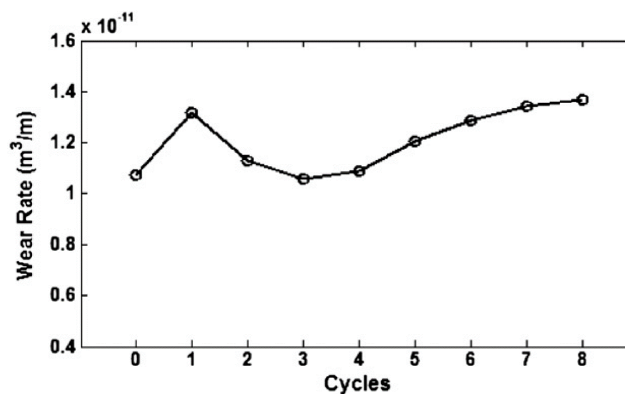

Figure 19. Variation of wear rate versus number of ARB cycles [125].

Wear observed in samples subjected to higher ARB cycles seem to occur by the mechanisms other than those usually observed in a lower number of cycles. After the third cycle, wear rate increased progressively due to the creation of high energy and unstable grain boundaries and high angle grain boundaries. These boundaries were reported to have low recrystallization temperature, they can easily rotate or coalesce when a large local strain is imposed (as in a wearing surface) leading to a rapid growth of the recrystallized grains at the subsurface. There would be a strain mismatch between the wearing surface with large recrystallized grains and the rest with non-equilibrium UFG structure. This is the cause for the delamination of the deformed layers that may result in high wear rates [126]. Darmiani et al. [127] investigated the wear resistance of ARBed pure Al/SiC$_P$ nanocomposite and

measured weight loss and friction coefficient. According to Figure 20a, it can be seen that the friction coefficient of a monolithic Al sample is larger than ARBed Al/SiC$_p$ composite and that increasing ARB cycles leads to reduced friction coefficient owing to the fact that SiC particles act as solid lubricant reducing the temperature at the contacts between the worn surface and the test pin.
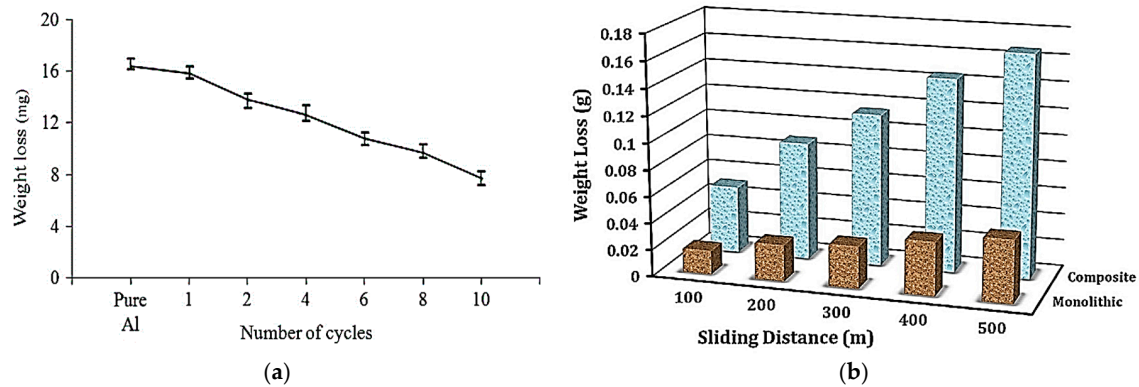

Figure 20. (**a**) Wear behavior of ARBed Al/SiC$_p$ nanocomposites processed by different rolling cycles, (**b**) wear behavior of monolithic material and seven-cycle ARBed Al/Al$_2$O$_3$ composite versus sliding distance [127].

Jamaati et al. [128] studied the wear behavior of nanostructured Al/Al$_2$O$_{3p}$ composite produced by an ARB process. Figure 20b shows the variations of weight loss versus the sliding distance of ARBed monolithic and composite samples. The ARB process causes an increase in weight loss of both monolithic and composite specimens compared with as-received strip, hence reducing wear resistance. Wear resistance was also decreased with an increase in number of ARB cycles. Wear contains a combination of three mechanisms of abrasion, adhesion and delamination; at a higher number of ARB cycles, delamination remains as the main wear mechanism. The nature of laminated structure helped further delamination during the wear test and that eliminates the grain size effect on the wear resistance. Although adhesive, abrasive and delaminating wear mechanisms simultaneously happened in the composite, surface damage resulting from the plastic deformation of ARBed composite was more widespread than the monolithic material. It was shown that both delamination and spalling mechanisms occurred in the composite, while it was just the delamination mechanism that occurred in the monolithic samples.

4.7. Corrosion

Materials with high microstructural defects, such as those UFG structures produced by ARB, usually have low corrosion resistance, however, it is still controversial to say that UFG materials have a poor corrosion resistance in comparison with their polycrystalline counterparts. The corrosion resistance of UFG materials depends on their alloy system and corrosive medium. Wei et al. [129] investigated the corrosion behavior of UFG Al–Mn alloy produced by an ARB operation. The results showed that the size and the number of pitting corrosion sites observed on the material are less than those coarse grain (CG) counterparts. The corrosion potential of UFG alloy was more positive than that of CG samples and the current density was much lower by ~33%. Immersed in 3.5% NaCl solution for 168 h, UFG Al alloy retained nearly unchanged tensile strength, while the degradation of total elongation was significant. Uniform pits formation was attributed to the energy balance between non-equilibrium grain boundaries and intragranular defects as well as reduction in particle size. The results showed that UFG Al–Mn alloy exhibit better resistance in than CG samples in 3.5% NaCl solution.

Darmiani et al. [130] studied the corrosion behavior of ARBed Al/SiCp nanocomposite and found that the corrosion resistance in both the surface and cross section of samples was enhanced for higher

number of ARB cycles. In addition, the corrosion resistance of surface samples was relatively better than those obtained from the cross samples for a specific ARB cycle. Kadkhodaee et al. [131] evaluated the corrosion of ARBed Al/nano-SiO2p nanocomposite sheets where the corrosion resistance strongly weakened after the first cycle but gradually resumed when the number of ARB cycles increased. The grain boundaries were found not to be active sites rather than grains causing the formation of more uniform and denser passive oxide layers on the specimens. In other research conducted by Fattah-Alhosseini et al. [132], the corrosion behavior of finely dispersed and highly uniform ARBed Al/B4C-SiCp hybrid composite in 3.5 wt.% NaCl solution was examined and it was shown that performing ARB leads to a lower corrosion current density of the fabricated hybrid composites as well as ARBed un-reinforced samples. Employing the ARB also led to a higher polarization resistance in all samples.

4.8. Fatigue

The response of materials under cyclic loading is one of the main materials selection criteria in both engineering and biomedical applications. Investigation of fatigue response of ARBed materials is, therefore, critical for validating their reliable use in various applications. In general, the fatigue limit has been recognized to be half of the tensile strength in smooth specimens [133–135]. Fatigue limit and fatigue strength usually become greater when the tensile strength improves. On the other hand, the dependence of the fatigue limit on the tensile strength is not necessarily linear and monotonic, so one has to prudently check the fatigue limit and strength when the tensile strength jumps markedly. As discussed in the previous section, ARB successfully enhances the tensile behavior of metallic materials, nonetheless, the fatigue crack resistance of the ARBed materials has rarely been investigated. Kwan and Wang [136] investigated the cyclic deformation behavior of UFG Cu processed by ARB and found that the conventional equiaxial grains are able to accommodate a fraction of the applied cyclic plastic strain through the development of slip bands within them due to the composite nature of the as-received ARBed Cu. Furthermore, grain coarsening was observed when the samples were subjected to cyclic loading both in load controlled and strain controlled tests. It was assumed that grain coarsening ultimately cause cyclic creep and cyclic softening behaviors observed via the increase in volume fraction of large-sized grains with a capability of developing slip bands within them.

Figure 21 shows a S-N diagram of the ARBed AA1050A/AA5005 composites with different ARB cycles and monolithic reference materials [137] wherein the fatigue life of the N4 composite (i.e., composite with 4 ARBed cycles) is very similar to the N8 composite at higher strain amplitudes. At smaller strain amplitudes, however, the N8 sample has significantly higher fatigue lives. Fatigue lives and damage mechanisms of both the N4 and N8 samples depend on the number and thickness of layers and thus the number of cycles, particularly at the lower amplitudes, where a noticeable grain coarsening of the AA1050A occurs. At higher amplitudes, the N8 sample is slightly shorter than the N4 sample whereas the fatigue life of the N8 one is considerably higher than the N4 samples at lower amplitudes. This can be attributed to the different crack growth behavior of the composite at different amplitudes. The fatigue life of the N12 composite is significantly improved compared to the N4 and N8. The samples fail at an equal number of fatigue cycles as the UFG AA5005 monomaterial sheet. Their evaluations revealed that the microstructure and the hardness of N12 composite is rather similar to that of the AA5005 monomaterial; thus, it is not surprising that the fatigue lives are rather similar as well. At higher total strain, the maximum stress in the AA1050A layers increase to magnitudes more than the yield strength of AA1050A; therefore, AA1050A experiences plastic deformation whereas the AA5005 layers does not.
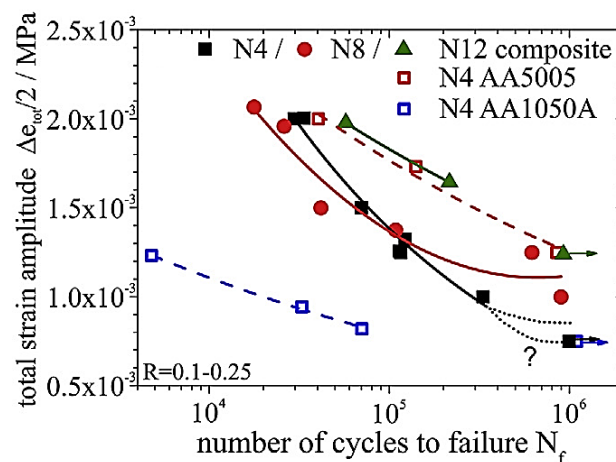
Figure 21. Total strain fatigue life diagram of the composites processed by different numbers of ARB cycles, ARB processed AA1050A and AA5005 mono-material sheets [137].

Besides the fatigue strength, Lin et al. [138] emphasized on the fatigue crack initiation and growth in ARBed IF steel. As the hardness increment has been empirically understood to enhance fatigue strength, they expected a positive effect of UFG microstructures on the fatigue crack resistance in terms of crack closure. Plasticity-induced crack closure (PICC), roughness-induced crack closure (RICC), transformation-induced crack closure, oxidation-induced crack closure, etc are some of the mechanisms of the fatigue crack closure; however, the degrees of PICC and RICC changes with UFG refinement. PICC occurs due to the formation of compressive residual stresses in the plastic wake while RICC is due to the deflection of crack paths and is related to the morphology of microstructures and grain sizes.

As demonstrated in Figure 22a, the fatigue limit for the CG and UFG steels was, respectively, 140 MPa and 300 MPa where the differences in the fatigue limit and life were attributed to hardness or tensile strength since the fatigue limit is governed by both yield stress and work hardening. Cycles to failure versus stress amplitude normalized by hardness is shown in Figure 22b and fatigue lives of the ARBed steel were practically identical to the CG steel.

Figure 22c shows the crack growth curves of the CG and ARBed steels, respectively, at the stress amplitudes of 180 MPa and 400 MPa. Fatigue crack growth (FCG) rate of the CG steel was lower compared to the UFG in short-crack region; but, in the long-crack region, the FCG rate of the UFG steel was lower in whole fatigue range at both stress amplitudes. The lower FCG rate in ARBed sample in long-crack region resulted in longer fatigue life at similar conditions compared with the CG specimen; the higher FCG rate of the CG steel was, in fact, attributed to the crack coalescence. The lower FCG rate of the CG steel in short-crack regime was attributed to RICC. Also, they stated that grain refinement might affect PICC behavior because of the change in crack tip plastic zone confirming the fact that the origin of the high FCG rates in the long-crack regime in the CG steel is associated with the crack coalescence, which is the consequence of low resistance to crack initiation. Additionally, delamination can decelerate FCG in the UFG steel resulting in a lower FCG rate in long-crack regime compared to the CG samples (Figure 22d).
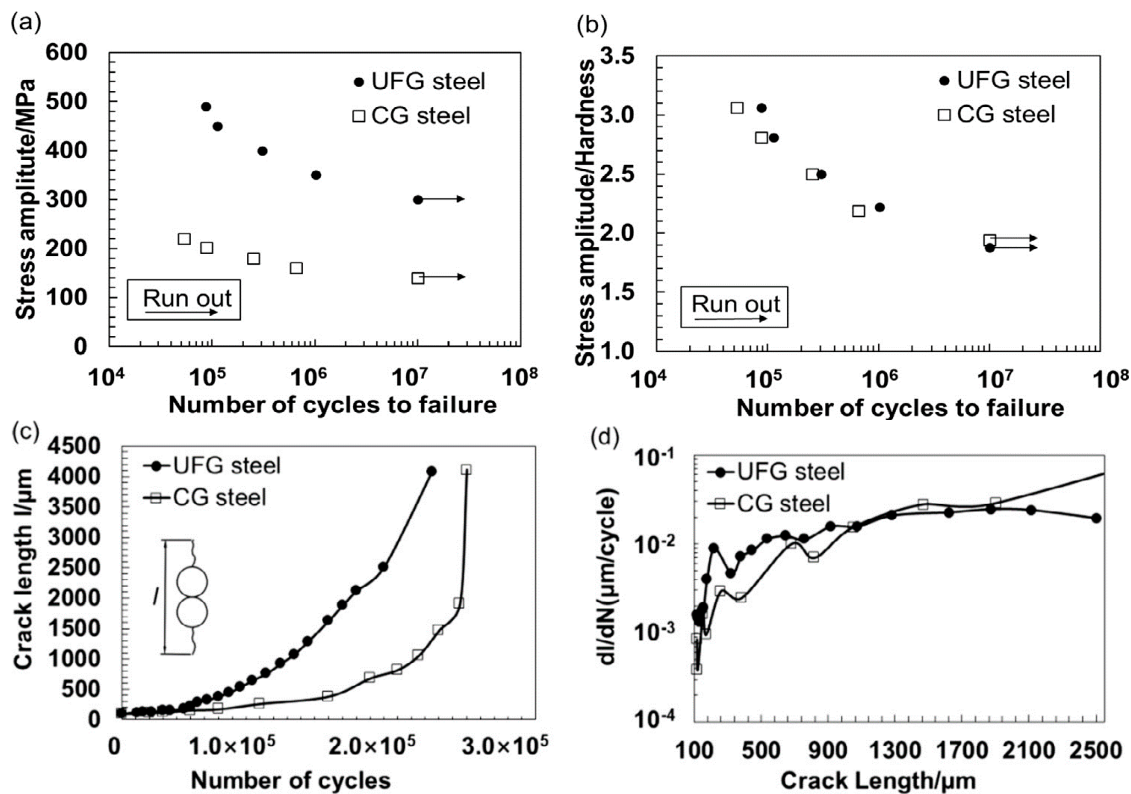
Figure 22. Up, (**a**) S-N curves of CG and UFG steels. (**b**) Number of cycles to failure plotted against stress amplitude normalized by hardness [138]; bottom, FCGR curves of the two steels at the same ratio between stress amplitude and hardness. (**c**) Crack length versus the number of cycles. (**d**) Crack growth rate versus crack length [138].

5. Computational Studies

The ARB process involves many variables, such as, material, rolling & post rolling treatment each having a considerable influence on the final product. Hence, it is desirable to have a computational framework to simulate and understand the ARB process in order to obtain optimized process parameters, to avoid trial and error experimental setups. To date, the efforts on the ARBed materials have mostly been devoted to experimental investigations and few computational studies have been reported in this regard [139–143]. Inoue and Tsuji [144], first correlate computational studies to ARB process parameters with the aim to quantify the strains in each component as well as to estimate the equivalent strain during a rolling process using finite element (FE) analysis. They used an FE method considering stress–strain relationships depending on strain rate and friction between rolls and sheet. The rolling condition of the ARB was verified through the embedded-pin method employed in their FE analysis. Using ABAQUS/Explicit, the exact magnitude of the total strains in each component and the equivalent strain during rolling were shown. According to Figure 23a, they showed that a considerably large equivalent strain, almost five times higher than that at the center, appears upon the surface. The equivalent strain at the surface of ARBed AA1100 without lubricant correspond to equivalent strain of five ARB cycles of lubricated samples. These quantitative strain analyses would be useful for analyzing the microstructural evolution of ARBed materials [145,146].

Roostaei et al. [147] applied a FE analysis to investigate the induced plastic strain during the ARB processing of AZ31 sheets using ABAQUS/Explicit as shown in Figure 23b; the effects of temperature and friction (between roller/sheet or sheet/sheet) on the through thickness deformation distributions were discussed. According to their results, the equivalent plastic strain increases when the friction coefficient is increased. As the temperature arises, the equivalent plastic strain diminishes. For AZ31 under this condition, they found that the temperature of 300 °C and friction coefficient of 0.35

compromised ARB processing parameters to achieve the highest homogeneous strain distribution accompanied by no significant grain growth. Similar FE investigations on the affecting parameters on deformation behavior during roll bonding were also carried out by Hosseini et al. [148] and Ebrahimi et al. [149].
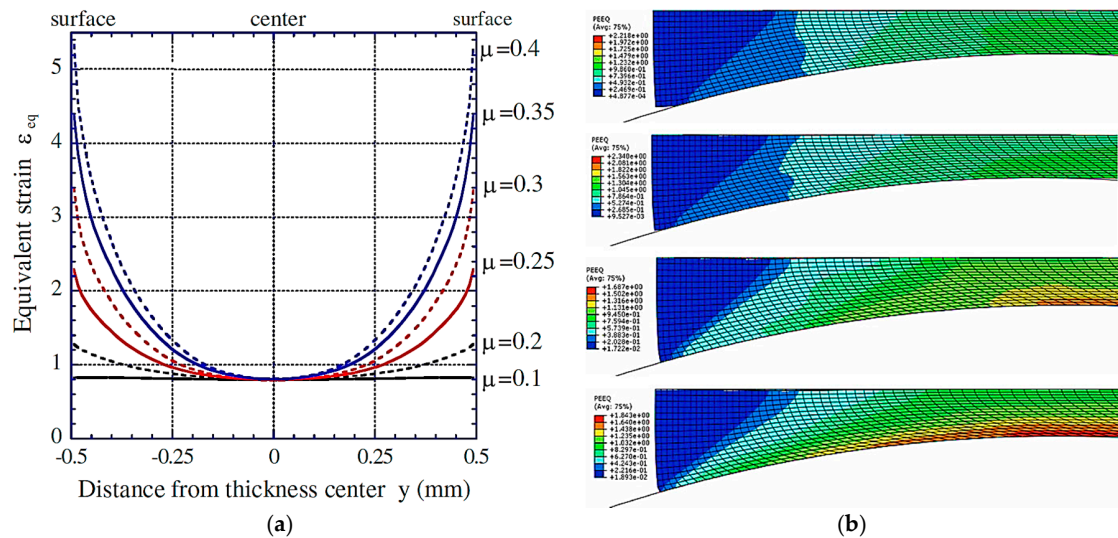

Figure 23. (**a**) equivalent strain through sheet thickness for varied friction coefficients [144], (**b**) the equivalent plastic strain contours obtained at 300 °C for different roller/sheet friction coefficients [147].

As it is relatively difficult to directly measure the plastic strain and stress distributions at the interface of the laminated composites in a hot-rolling process, Zhang et al. [150] used a FE analysis (Deform 2D software program) to characterize the bonding behavior of the laminated composites. Yu et al. [151] used a FE simulation to investigate the interface bonding quality of bimetallic foils produced by a combination of ARB and asymmetric rolling techniques. LS-DYNA software was employed to simulate the deformation of the bimetallic foils at various experimental conditions wherein a particular attention was placed on the interfacial bonding between AA1050 and AA6061 layers. The equivalent strain at the interface of the AA1050 and AA6061 layers was checked to reach a maximum value at a roll speed ratio of ~1.2–1.3, corresponding to a high-quality interfacial bonding. Prakash et al. [152] proposed a framework for multiple pass rolling using ABAQUS explicit poly-crystal texture model for studying visco-plastic self-consistent response to demonstrate the capabilities of this framework to predict the response of ARBed AA5754 alloy. Their simulations validated the solution framework and confirmed the development of a through thickness gradient of texture and anisotropy in an ARBed sheet after two cycles. A principal challenge in FE modeling of ARB process is growing the number of elements by a factor of two in each ARB cycle due to a large thickness reduction during each rolling cycle. The distortion of the mesh is also challenging and needs to be fixed.

Besides the efforts made on FE modelling of ARB process, some other studies were focused on predicting the mechanical properties of ARBed materials. Qiao and Starink [153] developed a grain refinement and strengthening model for oxide-free Al alloys processed by SPD to address ARBed Al alloys. Their model accurately predicted the grain refinement and hardness of an ARBed alloy. Milner et al. [154] simulated the evolution of material strength of an ARB-processed titanium alloy that was then validated using experimental data exhibiting an acceptable fit in whole range of ARB cycles. To further validate the model for a wider range of materials, five different materials were also investigated and the results confirmed the ability of the proposed method in predicting the strengthening behavior of all the considered materials. Reihanian and Naseri [155] proposed an analytical model for necking and fracture of the hard layer during the ARB substantiating that the critical strain for necking and fracture increased with increasing ARB ratio, strength coefficient ratio

and work-hardening exponent of the hard phase while it decreased with increasing the work-hardening exponent of the soft phase.

6. Concluding Remarks

Accumulative roll bonding is a severe plastic deformation process that involves rolling a stack of materials, sectioning into two halves, piling again and rolling repeatedly to produce an ultra-fine grain (UFG) structure. Here in this review, ARB process has been thoroughly reviewed and discussed starting with introducing different underlying mechanisms, influencing parameters and categorizing the ARB effects on different mechanical properties. The most influential parameters, such as those related to materials and process variables, are discussed. It was shown that the microstructural and surface features have a considerable effect on the final ARBed products, while the process conditions such as temperature, thickness reduction, friction, rolling speed, the type of reinforcing agent, and post-heat treatment parameters play key roles in determining the final performance. The effects of ARB on strength and ductility, thermal stability, superplasticity, vibration damping, fracture toughness, wear, corrosion, and cyclic behavior are also separately presented in this paper.

The ARB process has been simulated by a few computational methods; however, still a lot of research is required to understand more about this process owing to the complicated nature and synergistic effects of various processing parameters and governing underlying mechanisms. The effects of process parameters such as rolling stresses, frictions, temperatures and thermal issues, as well as non-linearities should be taken into investigations in future studies, leading to advanced materials and structures with desired properties.

Conflicts of Interest: The authors declare no conflict of interest.

References

1. SegaL, V. Materials processing by simple shear. *Mater. Sci. Eng.* **1995**, *197*, 157–164. [CrossRef]
2. Abdulov, R.; Valiev, R.; Krasilnikov, N. Formation of submicrometre-Grained structure in magnesium alloy due to high plastic strains. *J. Mater. Sci. Lett.* **1990**, *9*, 1445–1447. [CrossRef]
3. Ghalehbandi, S.; Fallahi-Arezodar, A.; Hosseini-Toudeshky, H. Fatigue crack growth resistance of 7075 Al alloy after equal channel angular pressing. *Fatigue Fract. Eng. Mater. Struct.* **2016**, *39*, 1517–1525. [CrossRef]
4. Horita, Z.; Fujinami, T.; Nemoto, M.; Langdon, T. Improvement of mechanical properties for Al alloys using equal-Channel angular pressing. *J. Mater. Process. Technol.* **2001**, *117*, 288–292. [CrossRef]
5. Valiev, R.Z.; Langdon, T.G. Principles of equal-Channel angular pressing as a processing tool for grain refinement. *Prog. Mater. Sci.* **2006**, *51*, 881–981. [CrossRef]
6. Ghalehbandi, S.M.; Arezoodar, A.F.; Hosseini-Toudeshky, H. Influence of aging on mechanical properties of equal channel angular pressed aluminum alloy 7075. *J. Proc. Inst. Mech. Eng. Part B* **2017**, *231*, 1803–1811. [CrossRef]
7. Zhilyaev, A.P.; Langdon, T.G. Using high-Pressure torsion for metal processing: Fundamentals and applications. *Prog. Mater. Sci.* **2008**, *53*, 893–979. [CrossRef]
8. Wei, Q.; Zhang, H.; Schuster, B.; Ramesh, K.; Valiev, R.; Kecskes, L.; Dowding, R.; Magness, L.; Cho, K. Microstructure and mechanical properties of super-Strong nanocrystalline tungsten processed by high-pressure torsion. *Acta Mater.* **2006**, *54*, 4079–4089. [CrossRef]
9. Edalati, K.; Fujioka, T.; Horita, Z. Microstructure and mechanical properties of pure Cu processed by high-pressure torsion. *Mater. Sci. Eng.* **2008**, *497*, 168–173. [CrossRef]
10. Tsuji, N.; Saito, Y.; Utsunomiya, H.; Tanigawa, S. Ultra-Fine grained bulk steel produced by accumulative roll-Bonding (ARB) process. *Scr. Mater.* **1999**, *40*, 795–800. [CrossRef]
11. Sheng, L.; Yang, F.; Xi, T.; Lai, C.; Ye, H. Influence of heat treatment on interface of Cu/Al bimetal composite fabricated by cold rolling. *Compos. Part B* **2011**, *42*, 1468–1473. [CrossRef]
12. Kitazono, K.; Sato, E.; Kuribayashi, K. Novel manufacturing process of closed-Cell aluminum foam by accumulative roll-Bonding. *Scr. Mater.* **2004**, *50*, 495–498. [CrossRef]

13. Fattahi, M.; Aghaei, V.N.; Dabiri, A.; Amirkhanlou, S.; Akhavan, S.; Fattahi, Y. Novel manufacturing process of nanoparticle/Al composite filler metals of tungsten inert gas welding by accumulative roll bonding. *Mater. Sci. Eng.* **2015**, *648*, 47–50. [CrossRef]

14. Sabetghadam-Isfahani, A.; Zalaghi, H.; Hashempour, S.; Fattahi, M.; Amirkhanlou, S.; Fattahi, Y. Fabrication and properties of ZrO2/AZ31 nanocomposite fillers of gas tungsten arc welding by accumulative roll bonding. *Arch. Civ. Mech. Eng.* **2016**, *16*, 397–402. [CrossRef]

15. Dhib, Z.; Guermazi, N.; Gaspérini, M.; Haddar, N. Cladding of low-Carbon steel to austenitic stainless steel by hot-Roll bonding: Microstructure and mechanical properties before and after welding. *Mater. Sci. Eng.* **2016**, *656*, 130–141. [CrossRef]

16. Bay, N. Cold welding. Part 1: Characteristics, bonding mechanisms, bond strength. *Met. Constr.* **1986**, *18*, 369–372.

17. Li, L.; Nagai, K.; Yin, F. Progress in cold roll bonding of metals. *Sci. Technol. Adv. Mater.* **2008**, *9*, 023001. [CrossRef] [PubMed]

18. Luo, J.G.; Acoff, V.L. Using cold roll bonding and annealing to process Ti/Al multi-Layered composites from elemental foils. *Mater. Sci. Eng.* **2004**, *379*, 164–172. [CrossRef]

19. Kwan, C.; Wang, Z.; Kang, S.B. Mechanical behavior and microstructural evolution upon annealing of the accumulative roll-bonding (ARB) processed Al alloy 1100. *Mater. Sci. Eng.* **2008**, *480*, 148–159. [CrossRef]

20. Mozaffari, A.; Hosseini, M.; Manesh, H.D. Al/Ni metal intermetallic composite produced by accumulative roll bonding and reaction annealing. *J. Alloys Compd.* **2011**, *509*, 9938–9945. [CrossRef]

21. Takata, N.; Yamada, K.; Ikeda, K.I.; Yoshida, F.; Nakashima, H.; Tsuji, N. Change in microstructure and texture during annealing of pure copper heavily deformed by accumulative roll bonding. *Mater. Trans.* **2007**, *48*, 2043–2048. [CrossRef]

22. Roostaei, A.A.; Zarei-Hanzaki, A.; Abedi, H.; Rokni, M. An investigation into the mechanical behavior and microstructural evolution of the accumulative roll bonded AZ31 Mg alloy upon annealing. *Mater. Des.* **2011**, *32*, 2963–2968. [CrossRef]

23. Talebian, M.; Alizadeh, M. Manufacturing Al/steel multilayered composite by accumulative roll bonding and the effects of subsequent annealing on the microstructural and mechanical characteristics. *Mater. Sci. Eng.* **2014**, *590*, 186–193. [CrossRef]

24. Kwan, C.; Wang, Z. Microstructure evolution upon annealing of accumulative roll bonding (ARB) 1100 Al sheet materials: Evolution of interface microstructures. *J. Mater. Sci. Lett.* **2008**, *43*, 5045–5051. [CrossRef]

25. Yoda, R.; Shibata, K.; Morimitsu, T.; Terada, D.; Tsuji, N. Formability of ultrafine-Grained interstitial-Free steel fabricated by accumulative roll-Bonding and subsequent annealing. *Scr. Mater.* **2011**, *65*, 175–178. [CrossRef]

26. Parks, J.M. Recrystallization welding. *Weld. J.* **1953**, 209–222. [CrossRef]

27. Semenov, A. The phenomenon of seizure and its investigation. *Wear* **1961**, *4*, 1–9. [CrossRef]

28. Vaidyanath, L.; Nicholas, M.; Milner, D. Pressure welding by rolling. *Bri. Weld. J.* **1959**, *6*, 13–28.

29. Mohamed, H.; Washburn, J. Mechanism of solid state pressure welding. *Weld. J.* **1975**, *8*, 302–310.

30. Pan, D.; Gao, K.; Yu, J. Cold roll bonding of bimetallic sheets and strips. *Mater. Sci. Technol.* **1989**, *5*, 934–939. [CrossRef]

31. Cantalejos, N. Morphology of the Interface of Roll-Bonded Aluminum. *J. Inst. Met.* **1972**, *100*, 20–23.

32. Jamaati, R.; Toroghinejad, M.R. Effect of friction, annealing conditions and hardness on the bond strength of Al/Al strips produced by cold roll bonding process. *Mater. Des.* **2010**, *31*, 4508–4513. [CrossRef]

33. Wu, H.-Y.; Lee, S.; Wang, J.Y. Solid-State bonding of iron-Based alloys, steel–Brass, and aluminum alloys. *J. Mater. Process. Technol.* **1998**, *75*, 173–179. [CrossRef]

34. Clemensen, C.; Juelstorp, O.; Bay, N. Cold welding. Part 3: Influence surface preparation on bond strength. *Met. Constr.* **1986**, *18*, 625–629.

35. Jamaati, R.; Toroghinejad, M.R. Manufacturing of high-Strength aluminum/alumina composite by accumulative roll bonding. *Mater. Sci. Eng.* **2010**, *527*, 4146–4151. [CrossRef]

36. Mehr, V.Y.; Toroghinejad, M.R.; Rezaeian, A. The effects of oxide film and annealing treatment on the bond strength of Al–Cu strips in cold roll bonding process. *Mater. Des.* **2014**, *53*, 174–181. [CrossRef]

37. Milner, D. Vaidyanath, L. Significance of surface preparation in cold pressure welding. *Met. Constr. Br. Weld. J.* **1960**, *7*, 1–6.

38. Jamaati, R.; Toroghinejad, M.R. The role of surface preparation parameters on cold roll bonding of aluminum strips. *J. Mater. Eng. Perform.* **2011**, *20*, 191–197. [CrossRef]

39. Sancaktar, E.; Gomatam, R. A study on the effects of surface roughness on the strength of single lap joints. *J. Adhes. Sci. Technol.* **2001**, *15*, 97–117. [CrossRef]

40. Kim, S.H.; Kim, H.W.; Euh, K.; Kang, J.H.; Cho, J.H. Effect of wire brushing on warm roll bonding of 6XXX/5XXX/6XXX aluminum alloy clad sheets. *Mater. Des.* **2012**, *35*, 290–295. [CrossRef]

41. Nicholas, M.; Milner, D. Pressure welding by rolling at elevated temperatures. *Br. Weld. J* **1961**, *8*, 375–383.

42. Quadir, M.; Wolz, A.; Hoffman, M.; Ferry, M. Influence of processing parameters on the bond toughness of roll-Bonded aluminium strip. *Scr. Mater.* **2008**, *58*, 959–962. [CrossRef]

43. Naseri, M.; Reihanian, M.; Borhani, E. Bonding behavior during cold roll-Cladding of tri-Layered Al/brass/Al composite. *J. Manuf. Process.* **2016**, *24*, 125–137. [CrossRef]

44. Hosseini, M.; Manesh, H.D. Bond strength optimization of Ti/Cu/Ti clad composites produced by roll-Bonding. *Mater. Des.* **2015**, *81*, 122–132. [CrossRef]

45. Ma, M.; Huo, P.; Liu, W.; Wang, G.; Wang, D. Microstructure and mechanical properties of Al/Ti/Al laminated composites prepared by roll bonding. *Mater. Sci. Eng.* **2015**, *636*, 301–310. [CrossRef]

46. Zhan, M.Y.; Li, Y.Y.; Chen, W.P. Improving mechanical properties of Mg-Al-Zn alloy sheets through accumulative roll-Bonding. *Trans. Nonferrous Metals Soc. China* **2008**, *18*, 309–314. [CrossRef]

47. Abbasi, M.; Sajjadi, S.A. Mechanical properties and interface evaluation of Al/AZ31 multilayer composites produced by ARB at different rolling temperatures. *J. Mater. Eng. Perform.* **2018**, *27*, 3508–3520. [CrossRef]

48. Xing, Z.; Kang, S.; Kim, H. Microstructural evolution and mechanical properties of the AA8011 alloy during the accumulative roll-Bonding process. *Metall. Mater. Trans. A* **2002**, *33*, 1521–1530. [CrossRef]

49. Quadir, M.; Al-Buhamad, O.; Bassman, L.; Ferry, M. Development of a recovered/recrystallized multilayered microstructure in Al alloys by accumulative roll bonding. *Acta Mater.* **2007**, *55*, 5438–5448. [CrossRef]

50. Miyajima, Y.; Uchiyama, M.; Adachi, H.; Fujii, T.; Onaka, S.; Kato, M. Effect of Roll-Bonding and Subsequent Annealing on Microstructure Evolution of Accumulative Roll Bonded Pure Copper. *Mater. Trans.* **2016**, *57*, 1411–1417. [CrossRef]

51. Jang, Y.; Kim, S.; Han, S.; Lim, C.; Goto, M. Tensile behavior of commercially pure copper sheet fabricated by 2-And 3-Layered accumulative roll bonding (ARB) process. *Metals Mater. Int.* **2008**, *14*, 171. [CrossRef]

52. Lee, S.H.; Utsunomiya, H.; Sakai, T. Microstructures and mechanical properties of ultra low carbon interstitial free steel severely deformed by a multi-Stack accumulative roll bonding process. *Mater. Trans.* **2004**, *45*, 2177–2181. [CrossRef]

53. Alizadeh, M.; Paydar, M. Fabrication of Al/SiCP composite strips by repeated roll-Bonding (RRB) process. *J. Alloys Compd.* **2009**, *477*, 811–816. [CrossRef]

54. Rezayat, M.; Akbarzadeh, A. Bonding behavior of Al–Al2O3 laminations during roll bonding process. *Mater. Des.* **2012**, *36*, 874–879. [CrossRef]

55. Jamaati, R.; Toroghinejad, M.R. High-Strength and highly-Uniform composite produced by anodizing and accumulative roll bonding processes. *Mater. Des.* **2010**, *31*, 4816–4822. [CrossRef]

56. Liu, C.; Wang, Q.; Jia, Y.; Zhang, B.; Jing, R.; Ma, M.; Jing, Q.; Liu, R. Evaluation of mechanical properties of 1060-Al reinforced with WC particles via warm accumulative roll bonding process. *Mater. Des.* **2013**, *43*, 367–372. [CrossRef]

57. Karimi, M.; Toroghinejad, M.R. An alternative method for manufacturing high-Strength CP Ti–SiC composites by accumulative roll bonding process. *Mater. Des.* **2014**, *59*, 494–501. [CrossRef]

58. Liu, C.; Wang, Q.; Jia, Y.; Zhang, B.; Jing, R.; Ma, M.; Jing, Q.; Liu, R. Effect of W particles on the properties of accumulatively roll-Bonded Al/W composites. *Mater. Sci. Eng.* **2012**, *547*, 120–124. [CrossRef]

59. Ahmadi, A.; Toroghinejad, M.R.; Najafizadeh, A. Evaluation of microstructure and mechanical properties of Al/Al2O3/SiC hybrid composite fabricated by accumulative roll bonding process. *Mater. Des.* **2014**, *53*, 13–19. [CrossRef]

60. Jamaati, R.; Toroghinejad, M.R.; Edris, H.; Salmani, M.R. Comparison of microparticles and nanoparticles effects on the microstructure and mechanical properties of steel-Based composite and nanocomposite fabricated via accumulative roll bonding process. *Mater. Des.* **2014**, *56*, 359–367. [CrossRef]

61. Kent, D.; Xiao, W.; Wang, G.; Yu, Z.; Dargusch, M. Thermal stability of an ultrafine grain β-Ti alloy. *Mater. Sci. Eng.* **2012**, *556*, 582–587. [CrossRef]

62. Gazder, A.A.; Hazra, S.S.; Pereloma, E.V. Annealing behaviour and mechanical properties of severely deformed interstitial free steel. *Mater. Sci. Eng.* **2011**, *530*, 492–503. [CrossRef]

63. Dhal, A.; Panigrahi, S.; Shunmugam, M. Precipitation phenomena, thermal stability and grain growth kinetics in an ultra-Fine grained Al 2014 alloy after annealing treatment. *J. Alloys Compd.* **2015**, *649*, 229–238. [CrossRef]

64. Morovvati, M.; Dariani, B.M. The effect of annealing on the formability of aluminum 1200 after accumulative roll bonding. *J. Manuf. Process.* **2017**, *30*, 241–254. [CrossRef]

65. Rezaei, M.R.; Toroghinejad, M.R.; Ashrafizadeh, F. Effects of ARB and ageing processes on mechanical properties and microstructure of 6061 aluminum alloy. *J. Mater. Process. Technol.* **2011**, *211*, 1184–1190. [CrossRef]

66. Xing, Z.; Kang, S.; Kim, H. Softening behavior of 8011 alloy produced by accumulative roll bonding process. *Scr. Mater.* **2001**, *45*, 597–604. [CrossRef]

67. Lee, S.; Saito, Y.; Sakai, T.; Utsunomiya, H. Microstructures and mechanical properties of 6061 aluminum alloy processed by accumulative roll-Bonding. *Mater. Sci. Eng.* **2002**, *325*, 228–235. [CrossRef]

68. Rezaei, M.R.; Toroghinejad, M.R.; Ashrafizadeh, F. Production of nano-Grained structure in 6061 aluminum alloy strip by accumulative roll bonding. *Mater. Sci. Eng.* **2011**, *529*, 442–446. [CrossRef]

69. Pirgazi, H.; Akbarzadeh, A.; Petrov, R.; Kestens, L. Microstructure evolution and mechanical properties of AA1100 aluminum sheet processed by accumulative roll bonding. *Mater. Sci. Eng.* **2008**, *497*, 132–138. [CrossRef]

70. Toroghinejad, M.R.; Ashrafizadeh, F.; Jamaati, R. On the use of accumulative roll bonding process to develop nanostructured aluminum alloy 5083. *Mater. Sci. Eng.* **2013**, *561*, 145–151. [CrossRef]

71. Su, L.; Lu, C.; Li, H.; Deng, G.; Tieu, K. Investigation of ultrafine grained AA1050 fabricated by accumulative roll bonding. *Mater. Sci. Eng.* **2014**, *614*, 148–155. [CrossRef]

72. Wang, T.; Zheng, H.; Wu, R.; Yang, J.; Ma, X.; Zhang, M. Preparation of Fine-Grained and High-Strength Mg–8Li–3Al–1Zn Alloy by Accumulative Roll Bonding. *Adv. Eng. Mater.* **2016**, *18*, 304–311. [CrossRef]

73. Lim, C.Y.; Han, S.Z.; Lee, S.H. Formation of nano-Sized grains in Cu and Cu− Fe− P alloys by accumulative roll bonding process. *Metals Mater. Int.* **2006**, *12*, 225–230. [CrossRef]

74. Shaarbaf, M.; Toroghinejad, M.R. Nano-Grained copper strip produced by accumulative roll bonding process. *Mater. Sci. Eng.* **2008**, *473*, 28–33. [CrossRef]

75. Song, H.; Kim, Y.; Nam, W. Mechanical properties of ultrafine grained 5052 Al alloy produced by accumulative roll-Bonding and cryogenic rolling. *Metals Mater. Int.* **2006**, *12*, 7–12. [CrossRef]

76. Ruppert, M.; Höppel, H.W.; Göken, M. Influence of cross-Rolling on the mechanical properties of an accumulative roll bonded aluminum alloy AA6014. *Mater. Sci. Eng.* **2014**, *597*, 122–127. [CrossRef]

77. Alvandi, H.; Farmanesh, K. Microstructural and mechanical properties of nano/ultra-Fine structured 7075 aluminum alloy by accumulative roll-Bonding process. *Proced. Mater. Sci.* **2015**, *11*, 17–23. [CrossRef]

78. Alvand, M.; Naseri, M.; Borhani, E.; Abdollah-Pour, H. Nano/ultrafine grained AA2024 alloy processed by accumulative roll bonding: A study of microstructure, deformation texture and mechanical properties. *J. Alloys Compd.* **2017**, *712*, 517–525. [CrossRef]

79. Terada, D.; Inoue, S.; Tsuji, N. Microstructure and mechanical properties of commercial purity titanium severely deformed by ARB process. *J. Mater. Sci.* **2007**, *42*, 1673–1681. [CrossRef]

80. Fattah-alhosseini, A.; Ansari, A.R.; Mazaheri, Y.; Karimi, M.; Haghshenas, M. An Investigation of mechanical properties in accumulative roll bonded nano-Grained pure titanium. *Mater. Sci. Eng.* **2017**, *688*, 218–224. [CrossRef]

81. Fattah-alhosseini, A.; Keshavarz, M.K.; Mazaheri, Y.; Ansari, A.R.; Karimi, M. Strengthening mechanisms of nano-Grained commercial pure titanium processed by accumulative roll bonding. *Mater. Sci. Eng.* **2017**, *693*, 164–169. [CrossRef]

82. Naseri, M.; Reihanian, M.; Borhani, E. A new strategy to simultaneous increase in the strength and ductility of AA2024 alloy via accumulative roll bonding (ARB). *Mater. Sci. Eng.* **2016**, *656*, 12–20. [CrossRef]

83. Zhang, R.; Acoff, V.L. Processing sheet materials by accumulative roll bonding and reaction annealing from Ti/Al/Nb elemental foils. *Mater. Sci. Eng.* **2007**, *463*, 67–73. [CrossRef]

84. Eizadjou, M.; Talachi, A.K.; Manesh, H.D.; Shahabi, H.S.; Janghorban, K. Investigation of structure and mechanical properties of multi-Layered Al/Cu composite produced by accumulative roll bonding (ARB) process. *Compos. Sci. Technol.* **2008**, *68*, 2003–2009. [CrossRef]

85. Eizadjou, M.; Manesh, H.D.; Janghorban, K. Microstructure and mechanical properties of ultra-Fine grains (UFGs) aluminum strips produced by ARB process. *J. Alloys Compd.* **2009**, *474*, 406–415. [CrossRef]

86. Ng, H.P.; Przybilla, T.; Schmidt, C.; Lapovok, R.; Orlov, D.; Höppel, H.W.; Göken, M. Asymmetric accumulative roll bonding of aluminium–Titanium composite sheets. *Mater. Sci. Eng.* **2013**, *576*, 306–315. [CrossRef]

87. Liu, C.; Zhang, B.; Yu, P.; Jing, R.; Ma, M.; Liu, R. Microstructures and mechanical properties of Al/Zn composites prepared by accumulative roll bonding and heat treatment. *Mater. Sci. Eng.* **2013**, *580*, 36–40. [CrossRef]

88. Mozaffari, A.; Manesh, H.D.; Janghorban, K. Evaluation of mechanical properties and structure of multilayered Al/Ni composites produced by accumulative roll bonding (ARB) process. *J. Alloys Compd.* **2010**, *489*, 103–109. [CrossRef]

89. Tayyebi, M.; Eghbali, B. Study on the microstructure and mechanical properties of multilayer Cu/Ni composite processed by accumulative roll bonding. *Mater. Sci. Eng.* **2013**, *559*, 759–764. [CrossRef]

90. Su, L.; Lu, C.; Tieu, A.K.; Deng, G.; Sun, X. Ultrafine grained AA1050/AA6061 composite produced by accumulative roll bonding. *Mater. Sci. Eng.* **2013**, *559*, 345–351. [CrossRef]

91. Sun, Y.; Tsuji, N.; Fujii, H.; Li, F. Cu/Zr nanoscaled multi-stacks fabricated by accumulative roll bonding. *J. Alloys Compd.* **2010**, *504*, 443–447. [CrossRef]

92. Dehsorkhi, R.N.; Qods, F.; Tajally, M. Investigation on microstructure and mechanical properties of Al–Zn composite during accumulative roll bonding (ARB) process. *Mater. Sci. Eng.* **2011**, *530*, 63–72. [CrossRef]

93. Alizadeh, M.; Samiei, M. Fabrication of nanostructured Al/Cu/Mn metallic multilayer composites by accumulative roll bonding process and investigation of their mechanical properties. *Mater. Des.* **2014**, *56*, 680–684. [CrossRef]

94. Ghalandari, L.; Mahdavian, M.; Reihanian, M. Microstructure evolution and mechanical properties of Cu/Zn multilayer processed by accumulative roll bonding (ARB). *Mater. Sci. Eng.* **2014**, *593*, 145–152. [CrossRef]

95. Chang, H.; Zheng, M.; Xu, C.; Fan, G.; Brokmeier, H.; Wu, K. Microstructure and mechanical properties of the Mg/Al multilayer fabricated by accumulative roll bonding (ARB) at ambient temperature. *Mater. Sci. Eng.* **2012**, *543*, 249–256. [CrossRef]

96. Yang, D.; Cizek, P.; Hodgson, P.; Wen, C.E. Ultrafine equiaxed-Grain Ti/Al composite produced by accumulative roll bonding. *Scr. Mater.* **2010**, *62*, 321–324. [CrossRef]

97. Alizadeh, M.; Talebian, M. Fabrication of Al/Cup composite by accumulative roll bonding process and investigation of mechanical properties. *Mater. Sci. Eng.* **2012**, *558*, 331–337. [CrossRef]

98. Lu, C.; Tieu, K.; Wexler, D. Significant enhancement of bond strength in the accumulative roll bonding process using nano-Sized SiO2 particles. *J. Mater. Process. Technol.* **2009**, *209*, 4830–4834. [CrossRef]

99. Amirkhanlou, S.; Rezaei, M.R.; Niroumand, B.; Toroghinejad, M.R. Refinement of microstructure and improvement of mechanical properties of Al/Al2O3 cast composite by accumulative roll bonding process. *Mater. Sci. Eng.* **2011**, *528*, 2548–2553. [CrossRef]

100. Ardakani, M.R.K.; Khorsand, S.; Amirkhanlou, S.; Nayyeri, M.J. Application of compocasting and cross accumulative roll bonding processes for manufacturing high-Strength, highly uniform and ultra-Fine structured Al/SiCp nanocomposite. *Mater. Sci. Eng.* **2014**, *592*, 121–127. [CrossRef]

101. Boesl, B.; Lahiri, D.; Behdad, S.; Agarwal, A. Direct observation of carbon nanotube induced strengthening in aluminum composite via in situ tensile tests. *Carbon* **2014**, *69*, 79–85. [CrossRef]

102. Melaibari, A.; Fathy, A.; Mansouri, M.; Eltaher, M. Experimental and numerical investigation on strengthening mechanisms of nanostructured Al-SiC composites. *J. Alloys Compd.* **2019**, *774*, 1123–1132. [CrossRef]

103. Wagih, A.; Fathy, A.; Ibrahim, D.; Elkady, O.; Hassan, M. Experimental investigation on strengthening mechanisms in Al-SiC nanocomposites and 3D FE simulation of Vickers indentation. *J. Alloys Compd.* **2018**, *752*, 137–147. [CrossRef]

104. Zhang, Z.; Chen, D. Contribution of Orowan strengthening effect in particulate-Reinforced metal matrix nanocomposites. *Mater. Sci. Eng.* **2008**, *483*, 148–152. [CrossRef]

105. Monazzah, A.H.; Pouraliakbar, H.; Jandaghi, M.R.; Bagheri, R.; Reihani, S.M.S. Influence of interfacial adhesion on the damage tolerance of Al6061/SiCp laminated composites. *Ceram. Int.* **2017**, *43*, 2632–2643. [CrossRef]

106. Luo, J.G.; Acoff, V.L. Processing gamma-Based TiAl sheet materials by cyclic cold roll bonding and annealing of elemental titanium and aluminum foils. *Mater. Sci. Eng.* **2006**, *433*, 334–342. [CrossRef]

107. Knudsen, F. Dependence of mechanical strength of brittle polycrystalline specimens on porosity and grain size. *J. Am. Ceram. Soc.* **1959**, *42*, 376–387. [CrossRef]

108. Hosseini, M.; Yazdani, A.; Manesh, H.D. Al 5083/SiCp composites produced by continual annealing and roll-bonding. *Mater. Sci. Eng.* **2013**, *585*, 415–421. [CrossRef]

109. Reihanian, M.; Hadadian, F.K.; Paydar, M. Fabrication of Al–2 vol% Al2O3/SiC hybrid composite via accumulative roll bonding (ARB): An investigation of the microstructure and mechanical properties. *Mater. Sci. Eng.* **2014**, *607*, 188–196. [CrossRef]

110. Toroghinejad, M.R.; Jamaati, R.; Nooryan, A.; Edris, H. Hybrid composites produced by anodizing and accumulative roll bonding (ARB) processes. *Ceram. Int.* **2014**, *40*, 10027–10035. [CrossRef]

111. Ana, S.A.; Reihanian, M.; Lotfi, B. Accumulative roll bonding (ARB) of the composite coated strips to fabricate multi-Component Al-Based metal matrix composites. *Mater. Sci. Eng.* **2015**, *647*, 303–312. [CrossRef]

112. Shamanian, M.; Mohammadnezhad, M.; Asgari, H.; Szpunar, J. Fabrication and characterization of Al–Al2O3–ZrC composite produced by accumulative roll bonding (ARB) process. *J. Alloys Compd.* **2015**, *618*, 19–26. [CrossRef]

113. Liu, X.; Wei, D.; Zhuang, L.; Cai, C.; Zhao, Y. Fabrication of high-Strength graphene nanosheets/Cu composites by accumulative roll bonding. *Mater. Sci. Eng.* **2015**, *642*, 1–6. [CrossRef]

114. Reihanian, M.; Shahmansouri, M.J.; Khorasanian, M. High strength Al with uniformly distributed Al2O3 fragments fabricated by accumulative roll bonding and plasma electrolytic oxidation. *Mater. Sci. Eng.* **2015**, *640*, 195–199. [CrossRef]

115. Rezayat, M.; Akbarzadeh, A.; Owhadi, A. Production of high strength Al–Al2O3 composite by accumulative roll bonding. *Compos. Part A* **2012**, *43*, 261–267. [CrossRef]

116. Park, K.T.; Kwon, H.J.; Kim, W.J.; Kim, Y.S. Microstructural characteristics and thermal stability of ultrafine grained 6061 Al alloy fabricated by accumulative roll bonding process. *Mater. Sci. Eng.* **2001**, *316*, 145–152. [CrossRef]

117. Slamova, M.; Homola, P.; Karlik, M. Thermal stability of twin-Roll cast Al–Fe–Mn–Si sheets accumulative roll bonded at different temperatures. *Mater. Sci. Eng.* **2007**, *462*, 106–110. [CrossRef]

118. Tsuji, N.; Shiotsuki, K.; Saito, Y. Superplasticity of ultra-Fine grained Al–Mg alloy produced by accumulative roll-Bonding. *Mater. Trans.* **1999**, *40*, 765–771. [CrossRef]

119. Koizumi, Y.; Ueyama, M.; Tsuji, N.; Minamino, Y.; Ota, K.I. High damping capacity of ultra-Fine grained aluminum produced by accumulative roll bonding. *J. Alloys Compd.* **2003**, *355*, 47–51. [CrossRef]

120. Emadoddin, E.; Tajally, M.; Masoumi, M. Damping behavior of Al/SiCP multilayer composite manufactured by roll bonding. *Mater. Des.* **2012**, *42*, 334–338. [CrossRef]

121. Zheng, W.; Gao, Y.; Wang, X.; Lu, H.; Zeng, L.; Fang, Q. High strength and damping capacity of LLZNO/Al composites fabricated by accumulative roll bonding. *Mater. Sci. Eng.* **2017**, *689*, 306–312. [CrossRef]

122. Rahmatabadi, D.; Hashemi, R.; Mohammadi, B.; Shojaee, T. Experimental evaluation of the plane stress fracture toughness for ultra-Fine grained aluminum specimens prepared by accumulative roll bonding process. *Mater. Sci. Eng.* **2017**, *708*, 301–310. [CrossRef]

123. Cepeda-Jiménez, C.; Hidalgo, P.; Pozuelo, M.; Ruano, O.A.; Carreño, F. Influence of constituent materials on the impact toughness and fracture mechanisms of hot-Roll-Bonded aluminum multilayer laminates. *Metall. Mater. Trans. A* **2010**, *41*, 61. [CrossRef]

124. Pippan, R.; Hohenwarter, A. The importance of fracture toughness in ultrafine and nanocrystalline bulk materials. *Mater. Res. Lett.* **2016**, *4*, 127–136. [CrossRef] [PubMed]

125. Talachi, A.K.; Eizadjou, M.; Manesh, H.D.; Janghorban, K. Wear characteristics of severely deformed aluminum sheets by accumulative roll bonding (ARB) process. *Mater. Charact.* **2011**, *62*, 12–21. [CrossRef]

126. Kim, Y.S.; Ha, J.; Shin, D.H. Sliding wear characteristics of ultrafine-Grained non-Strain-Hardening aluminum-Magnesium alloys, Materials science forum. *Trans Tech. Publ.* **2005**, *475*, 401–404.

127. Darmiani, E.; Danaee, I.; Golozar, M.; Toroghinejad, M.; Ashrafi, A.; Ahmadi, A. Reciprocating wear resistance of Al–SiC nano-Composite fabricated by accumulative roll bonding process. *Mater. Des.* **2013**, *50*, 497–502. [CrossRef]

128. Jamaati, R.; Naseri, M.; Toroghinejad, M.R. Wear behavior of nanostructured Al/Al2O3 composite fabricated via accumulative roll bonding (ARB) process. *Mater. Des.* **2014**, *59*, 540–549. [CrossRef]

129. Wei, W.; Wei, K.X.; Du, Q.B. Corrosion and tensile behaviors of ultra-Fine grained Al–Mn alloy produced by accumulative roll bonding. *Mater. Sci. Eng.* **2007**, *454*, 536–541. [CrossRef]

130. Darmiani, E.; Danaee, I.; Golozar, M.; Toroghinejad, M. Corrosion investigation of Al–SiC nano-composite fabricated by accumulative roll bonding (ARB) process. *J. Alloys Compd.* **2013**, *552*, 31–39. [CrossRef]

131. Kadkhodaee, M.; Babaiee, M.; Manesh, H.D.; Pakshir, M.; Hashemi, B. Evaluation of corrosion properties of Al/nanosilica nanocomposite sheets produced by accumulative roll bonding (ARB) process. *J. Alloys Compd.* **2013**, *576*, 66–71. [CrossRef]

132. Fattah-Alhosseini, A.; Naseri, M.; Alemi, M. Corrosion behavior assessment of finely dispersed and highly uniform Al/B4C/SiC hybrid composite fabricated via accumulative roll bonding process. *J. Manuf. Process.* **2016**, *22*, 120–126. [CrossRef]

133. Suresh, S. *Fatigue of Materials*; Cambridge University Press: Cambridge, UK, 1998.

134. Chapetti, M.; Miyata, H.; Tagawa, T.; Miyata, T.; Fujioka, M. Fatigue strength of ultra-Fine grained steels. *Mater. Sci. Eng.* **2004**, *381*, 331–336. [CrossRef]

135. Vinogradov, A.; Hashimoto, S.; Kopylov, V. Enhanced strength and fatigue life of ultra-Fine grain Fe–36Ni Invar alloy. *Mater. Sci. Eng.* **2003**, *355*, 277–285. [CrossRef]

136. Kwan, C.C.; Wang, Z. Cyclic deformation behavior of ultra-Fine grained copper processed by accumulative roll-Bonding. *Proced. Eng.* **2010**, *2*, 101–110. [CrossRef]

137. Kümmel, F.; Hausöl, T.; Höppel, H.W.; Göken, M. Enhanced fatigue lives in AA1050A/AA5005 laminated metal composites produced by accumulative roll bonding. *Acta Mater.* **2016**, *120*, 150–158. [CrossRef]

138. Lin, X.; Koyama, M.; Gao, S.; Tsuji, N.; Tsuzaki, K.; Noguchi, H. Resistance to mechanically small fatigue crack growth in ultrafine grained interstitial-Free steel fabricated by accumulative roll-Bonding. *Int. J. Fatigue* **2019**, *118*, 117–125. [CrossRef]

139. Galantucci, L.; Tricarico, L. Thermo-Mechanical simulation of a rolling process with an FEM approach. *J. Mater. Process. Technol.* **1999**, *92*, 494–501. [CrossRef]

140. Min, W.; He, Y.; Sun, Z.C.; Guo, L.G.; Ou, X.Z. Dynamic explicit FE modeling of hot ring rolling process. *Trans. Nonferrous Metals Soc. China* **2006**, *16*, 1274–1280.

141. Mori, K.; Osakada, K.; Oda, T. Simulation of plane-Strain rolling by the rigid-Plastic finite element method. *Int. J. Mech. Sci.* **1982**, *24*, 519–527. [CrossRef]

142. Jiang, Z.; Tieu, A.; Zhang, X.; Lu, C.; Sun, W. Finite element simulation of cold rolling of thin strip. *J. Mater. Process. Technol.* **2003**, *140*, 542–547. [CrossRef]

143. Beaudoin, A.J.; Mathur, K.; Dawson, P.; Johnson, G. Three-Dimensional deformation process simulation with explicit use of polycrystal plasticity models. *Int.l J. Plast.* **1993**, *9*, 833–860. [CrossRef]

144. Inoue, T.; Tsuji, N. Quantification of strain in accumulative roll-Bonding under unlubricated condition by finite element analysis. *Comput. Mater. Sci.* **2009**, *46*, 261–266. [CrossRef]

145. Tseng, H.C.; Hung, C.; Huang, C.C. An analysis of the formability of aluminum/copper clad metals with different thicknesses by the finite element method and experiment. *Int. J. Adv. Manuf. Technol.* **2010**, *49*, 1029–1036. [CrossRef]

146. Inoue, T.; Yanagida, A.; Yanagimoto, J. Finite element simulation of accumulative roll-Bonding process. *Mater. Letters* **2013**, *106*, 37–40. [CrossRef]

147. Roostaei, A.A.; Zarei-Hanzaki, A.; Parsa, M.; Fatemi-Varzaneh, S. An analysis to plastic deformation behavior of AZ31 alloys during accumulative roll bonding process. *J. Mater. Sci. Lett.* **2010**, *45*, 4494–4500. [CrossRef]

148. Hosseini, M.; Pardis, N.; Manesh, H.D.; Abbasi, M.; Kim, D.I. Structural characteristics of Cu/Ti bimetal composite produced by accumulative roll-Bonding (ARB). *Mater. Des.* **2017**, *113*, 128–136. [CrossRef]

149. Ebrahimi, S.S.; Dehghani, K.; Aghazadeh, J.; Ghasemian, M.; Zangeneh, S. Investigation on microstructure and mechanical properties of Al/Al-Zn-Mg–Cu laminated composite fabricated by accumulative roll bonding (ARB) process. *Mater. Sci. Eng.* **2018**, *718*, 311–320. [CrossRef]

150. Zhang, X.; Yang, T.; Castagne, S.; Gu, C.; Wang, J. Proposal of bond criterion for hot roll bonding and its application. *Mater. Des.* **2011**, *32*, 2239–2245. [CrossRef]

151. Yu, H.; Tieu, A.K.; Lu, C.; Godbole, A. An investigation of interface bonding of bimetallic foils by combined accumulative roll bonding and asymmetric rolling techniques. *Metall. Mater. Trans. A* **2014**, *45*, 4038–4045. [CrossRef]

152. Prakash, A.; Nöhring, W.; Lebensohn, R.; Höppel, H.; Bitzek, E. A multiscale simulation framework of the accumulative roll bonding process accounting for texture evolution. *Mater. Sci. Eng.* **2015**, *631*, 104–119. [CrossRef]

153. Qiao, X.G.; Starink, M.J. Prediction of hardness of Al alloys processed by accumulative roll bonding. *Mater. Sci. Eng.* **2012**, *531*, 45–50. [CrossRef]

154. Milner, J.L.; Bunget, C.; Abu-Farha, F.; Kurfess, T.; Hammond, V.H. Modeling tensile strength of materials processed by accumulative roll bonding. *J. Manuf. Process.* **2013**, *15*, 219–226. [CrossRef]

155. Reihanian, M.; Naseri, M. An analytical approach for necking and fracture of hard layer during accumulative roll bonding (ARB) of metallic multilayer. *Mater. Des.* **2016**, *89*, 1213–1222. [CrossRef]